AFRL-IF-RS-TR-2002-96
In-House Final Technical Report
May 2002

INTERFERENCE MITIGATION IN SPREAD SPECTRUM SYSTEMS USING LAPPED TRANSFORMS

Michael J. Medley

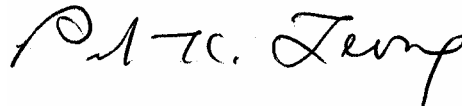*APPROVED FOR PUBLIC RELEASE; DISTRIBUTION UNLIMITED.*

AIR FORCE RESEARCH LABORATORY
INFORMATION DIRECTORATE
ROME RESEARCH SITE
ROME, NEW YORK

This report has been reviewed by the Air Force Research Laboratory, Information Directorate, Public Affairs Office (IFOIPA) and is releasable to the National Technical Information Service (NTIS). At NTIS it will be releasable to the general public, including foreign nations.

AFRL-IF-RS-TR-2002-96 has been reviewed and is approved for publication.

APPROVED: PETER K. LEONG, Chief
Information Connectivity Branch
Information Grid Division
Information Directorate

FOR THE DIRECTOR: WARREN H. DEBANY JR.
Technical Advisor
Information Grid Division
Information Directorate

1. AGENCY USE ONLY (Leave blank)	2. REPORT DATE May 2002	3. REPORT TYPE AND DATES COVERED In-House Final, Dec 96 – Dec 99

4. TITLE AND SUBTITLE INTERFERENCE MITIGATION IN SPREAD SPECTRUM SYSTEMS USING LAPPED TRANSFORMS	5. FUNDING NUMBERS PE - 62702F PR - 4519 TA - 42 WU - 96
6. AUTHOR(S) Michael J. Medley	

7. PERFORMING ORGANIZATION NAME(S) AND ADDRESS(ES) AFRL/IFGC 525 Brooks Road Rome, NY 13441-4505	8. PERFORMING ORGANIZATION REPORT NUMBER AFRL-IF-RS-TR-2002-96

9. SPONSORING / MONITORING AGENCY NAME(S) AND ADDRESS(ES) AFRL/IFGC 525 Brooks Road Rome, NY 13441-4505	10. SPONSORING / MONITORING AGENCY REPORT NUMBER AFRL-IF-RS-TR-2002-96

11. SUPPLEMENTARY NOTES
AFRL Project Engineer: Michael J. Medley/IFGC/315-330-4830

12a. DISTRIBUTION / AVAILABILITY STATEMENT APPROVED FOR PUBLIC RELEASE; DISTRIBUTION UNLIMITED.	12b. DISTRIBUTION CODE

13. ABSTRACT *(Maximum 200 Words)*

In this report, linear and non-linear transform domain filtering techniques are examined and proposed as a means of enhancing the inherent interference immunity associated with direct sequence spread spectrum communication receivers. This analysis begins with a review of block transform domain Wiener filters and is further developed in the lapped transform domain. The latter part of this report addresses the use of lapped transforms to transform the received data signal into the transform domain wherein adaptive excision is performed. System performance results are presented for a variety of channel conditions and compared to those obtained using orthonormal block transforms. These results demonstrate the improved performance and increased robustness with respect to jammer frequency and bandwidth of lapped transform domain excision techniques relative to similar algorithms based on non-weighted block transforms.

14. SUBJECT TERMS cosine-modulated filter banks, spread spectrum communications, transform domain Wiener filtering, excision, detection, interference suppression, lapped transforms, minimum mean-square error			15. NUMBER OF PAGES 56
			16. PRICE CODE

17. SECURITY CLASSIFICATION OF REPORT UNCLASSIFIED	18. SECURITY CLASSIFICATION OF THIS PAGE UNCLASSIFIED	19. SECURITY CLASSIFICATION OF ABSTRACT UNCLASSIFIED	20. LIMITATION OF ABSTRACT UL

Contents

List of Figures

1   Introduction

In an effort to transmit information over communications channels corrupted by narrow-band interference, both military and commercial applications frequently rely on the use of spread spectrum communications systems. In general, spread spectrum signaling refers to a class of digital modulation techniques which produce a transmitted frequency spectrum much larger than that of the information being sent. While this may seem wasteful of bandwidth, the process of "spreading" and "despreading" the spectrum produces some important, desirable properties such as interference rejection and low power spectral density.

Although an arbitrary level of protection against narrow-band interferers can be obtained by designing the spread signal with sufficiently large processing gain, which is the ratio of spread to non-spread data bandwidth, practical considerations such as transmitter/receiver complexity and available frequency spectrum often serve to limit reasonably attainable transmit bandwidth. As a result, it is often necessary to employ signal processing techniques, such as adaptive Wiener filtering [13, 16, 42, 35] and transform domain excision [11, 28, 29, 30] to augment the processing gain of the spread spectrum signal without increasing its bandwidth. Of the many different spread spectrum modulation techniques employed in contemporary communications systems [3, 9], only direct sequence spread spectrum (DSSS) is considered here.

In this work, narrow-band interference suppression via transform domain Wiener filtering and transform domain excision are examined. Both block transforms, such as the discrete Fourier transform (DFT) and the discrete cosine transform (DCT), along with lapped transforms are considered. In contrast to less complex interference mitigation techniques such as transform domain excision and notch filtering [1, 2, 7, 10, 12, 26, 38, 40, 41], transform domain Wiener filtering is a technique that minimizes the mean-square error (MSE) between the estimate of the received data bit and its actual value and serves as a benchmark against which other interference mitigation
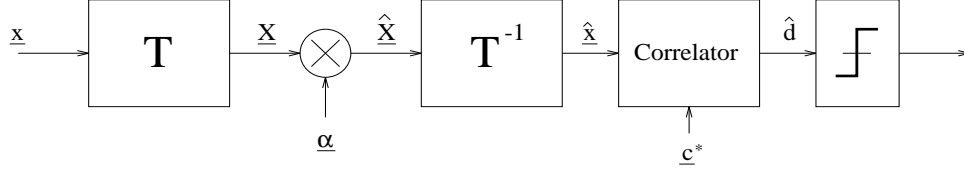
Figure 1: Discrete-time receiver employing pre-correlation transform domain filtering.

algorithms can be compared and evaluated.

In the following section, orthonormal block and lapped transforms are reviewed. Pre- and post-correlation transform domain Wiener filters are subsequently discussed in Section 2.2 wherein optimal transform domain filter coefficients minimizing the MSE between the estimated data bit and its actual value are derived. An analysis of the bit error rate achieved via transform domain Wiener filtering is presented in Section 2.3 with the corresponding analytical and simulation results given in Section 2.4. Section 3 demonstrates how LTs can be used in a transform domain exciser. Section 3.1 presents an analysis of the BER performance of these transform domain excisers in the presence of tone and narrow-band Gaussian interference with the corresponding results illustrated in Section 3.2. To demonstrate the performance improvement realized using LTs, these results are depicted alongside those obtained using traditional block transform domain excision techniques. A brief summary of the analysis and results presented herein is given in Section 4.

2 Optimal Linear Filtering in the Transform Domain

Direct sequence receivers demodulate, despread and detect the received data signal in an effort to reconstruct or estimate the originally transmitted message symbol; it is typically assumed that these receivers have a priori knowledge of the spreading sequence. To make a bit decision, the receiver multiplies the received signal, $x[n]$,

by a locally-generated, synchronized copy of the spreading sequence and integrates the result over a data bit period. Figure 1 illustrates a generic discrete-time receiver employing arbitrary transform domain filtering. In this figure, T and T^{-1} denote arbitrary forward and inverse N-point transforms, respectively, and the weighting vector, $\underline{\alpha}$, where $\{\alpha_k, \ 0 \leq k \leq N-1\}$, represents the appropriate transform domain filter coefficients. The resynthesized, or filtered, received data vector, $\underline{\hat{x}}$, is subsequently correlated with the reference spreading code to produce the appropriate decision variable. This receiver is referred to as a "pre-correlation" receiver since the filtering operation precedes the correlation of the signal with the reference code. It should be clear from this figure that if the identity transform is used, this receiver reduces to a conventional time domain correlator for the known reference code and the time-weighted signal, $\hat{x}[n]$.

Although practical estimation of the transform domain Wiener filter coefficients can be achieved by any of a number of adaptive techniques [8, 45], the least mean square (LMS) algorithm is most commonly employed due to its low computational complexity. As a result, transform domain LMS algorithms have been well documented in the literature [4, 8, 15, 21, 32]. Most of the analysis contained in these and related works includes the use of power normalization in an effort to reduce the spread, or max/min ratio, of the eigenvalues associated with the input autocorrelation matrix and, thus, improve convergence performance. As demonstrated in [4], the frequency response associated with each of the transform basis vectors, or subbands, directly affects algorithmic convergence — in the presence of narrow-band waveforms, subband filters with better spectral resolution and stopband attenuation yield improved convergence rates. Although further discussion regarding adaptive algorithms is beyond the scope of this work, improvement in algorithmic convergence rates, as well as the need for an optimal performance benchmark, serve as motivation for the derivation of Wiener filter coefficients for various transforms with narrow-band basis vectors. In

this work, only the fundamental analysis of transform domain Wiener filters using various transforms and implementations is discussed; extensions of this analysis to transform domain LMS algorithms is treated in [22] and [25].

Since the length of the transform basis vectors directly affects spectral resolution and stopband attenuation, the opportunity to choose longer basis vectors, as offered by filter banks, may be used to improve transform domain resolution and, ultimately, enhance algorithmic performance and narrow-band interference suppression capability. Fortunately, there exist efficient filter bank structures that allow the longer filters to be used while only moderately increasing the number of required arithmetic operations [19].

Recent efforts in filter bank design have focused on the development of perfect reconstruction (PR) filter banks with higher order subband filters [17, 20]. These filters, whose length, L, is equal to some even integer multiple of the number of filter bank subbands, M, i.e. $L = 2KM$, where K is the *overlapping factor*, are implemented as the basis vectors of *lapped transforms* (LT) [19]. Modulated lapped transforms (MLT) are considered as a LT subclass for which $K = 1$. Longer extensions of the subband filters in which the overlapping factor is greater than two, i.e. $K \geq 2$, are generally referred to as extended lapped transforms (ELT) [19].

2.1 Signal Analysis Using Linear Transforms

Practical solutions to many communications problems often require an efficient means of identifying, compressing and/or manipulating information bearing waveforms. Accordingly, an invertible linear transform is commonly employed to map discrete-time signals into a new domain wherein key features are succinctly represented and processed. Linear transforms characterized by narrow-band basis vectors, such as the DFT, the DCT and cosine-modulated filter banks, are well-suited for narrow-band signal analysis and are often used to resolve the various components of bandlim-

4

ited waveforms. The level of frequency domain resolution and, hence, quality of the analysis depends on how well the basis vectors represent the signal of interest — a good match typically results in efficient transform domain representation while a poor match indicates that the proposed transform is most likely unsuitable for the given input.

2.1.1 Orthonormal Block (Unitary) Transforms

Throughout the following sections, discrete-time signals are treated as vectors in linear space. Therefore, unless otherwise noted, discrete-time signals, such as $x[n]$, are treated as N-dimensional vectors, and are denoted in column vector format, i.e.

$$\underline{x} = [x[0]\ x[1] \dots x[N-1]]^T = [x_0\ x_1 \dots x_{N-1}]^T,$$

with the indices for individual elements labeled from 0 to $N-1$.

Denoting the $N \times N$ block transformation matrix as $\mathbf{\Phi}$, the time and transform domain signal representations in vector notation are written as

$$\underline{x} = \mathbf{\Phi}^T \underline{X} \quad \text{and} \quad \underline{X} = \mathbf{\Phi}^* \underline{x}, \tag{1}$$

respectively. Clearly, for invertible transformations, these equations imply that the transformation matrix $\mathbf{\Phi}$ is a *unitary* matrix, i.e. $\mathbf{\Phi}^\dagger \mathbf{\Phi} = \mathbf{\Phi} \mathbf{\Phi}^\dagger = \mathbf{I}$, where † denotes the complex conjugate transpose operator and $\mathbf{I}$ is the N-dimensional identity matrix.

2.1.2 Modulated Lapped Transforms

Inherent in the design of lapped transforms is the satisfaction of the *perfect reconstruction* (PR) criterion, which implies that for an input sequence, $x[n]$, the reconstructed signal samples, $\hat{x}[n]$, are equal to the original values to within a constant scale and delay adjustment, i.e.

$$\hat{x}[n] = cx[n-n'],$$

where c and n' are constants. Like block transforms, LTs can be represented by a transformation matrix, $\boldsymbol{\Psi}$, whose rows are the individual basis vectors. Whereas the transformation matrix for a block unitary transform is square, the LT transformation matrix, as considered here, is real with dimensions $M \times 2KM$.

Viewing the LT transformation matrix as an infinite-dimensional block diagonal extension of $\boldsymbol{\Psi}$, i.e. $\tilde{\boldsymbol{\Psi}} = \mathrm{diag}\,(\,\cdots\,\boldsymbol{\Psi}\,\boldsymbol{\Psi}\,\boldsymbol{\Psi}\,\cdots\,)$, and considering only real signals and transforms, PR for lapped transforms can be achieved if and only if [19]

$$\tilde{\boldsymbol{\Psi}}\tilde{\boldsymbol{\Psi}}^T = \mathbf{I} \qquad \Leftrightarrow \qquad \tilde{\boldsymbol{\Psi}}^T\tilde{\boldsymbol{\Psi}} = \mathbf{I}. \tag{2}$$

In this case, $\mathrm{diag}\,(\cdot)$ denotes a matrix whose block diagonal submatrices correspond to those given in the argument; the superscript T denotes the matrix transpose operation. These equations indicate the necessary conditions for orthogonality between the LT basis vectors and the conditions required for orthogonality of the overlapping "tails" of the basis vectors.

As in [18, 19], MLTs are considered here as a subset of LTs with $K = 1$. The basic premise of the MLT is to use a $2M$-tap lowpass filter as a subband filter prototype which is shifted in frequency to produce a set of orthogonal bandpass FIR filters spanning the frequency range of interest. Denoting the lowpass prototype as $h[n]$, the sinusoidally modulated basis vectors can be expressed as [19]

$$\psi_k[n] = h[n]\sqrt{\frac{2}{M}}\cos\left[\left(n + \frac{M+1}{2}\right)\left(k + \frac{1}{2}\right)\frac{\pi}{M}\right], \tag{3}$$

where $0 \le n \le 2M - 1$ and $0 \le k \le M - 1$.

Of central importance to the development of the MLT is the design of the lowpass prototype, $h[n]$. To meet the PR requirements imposed by (2), $h[n]$ must satisfy the following requirements [19],

$$h[2M - 1 - n] = h[n] \qquad 0 \le n \le M - 1 \tag{4}$$

and

$$h^2[n] + h^2[n + M] = 1 \qquad 0 \le n \le M/2 - 1. \tag{5}$$
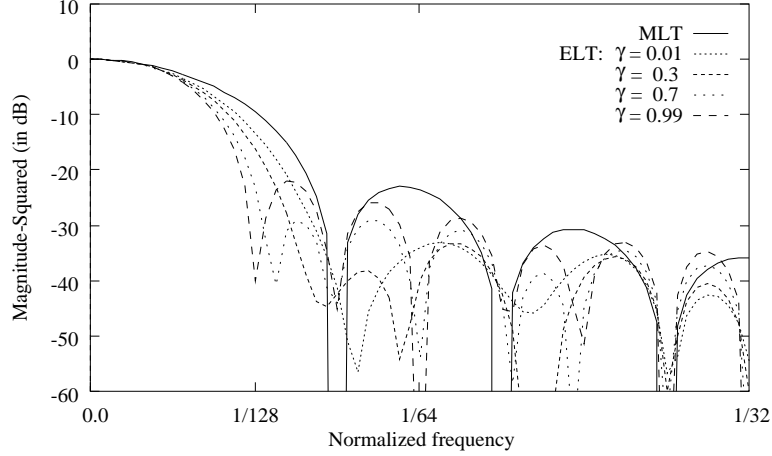
Figure 2: MLT and ELT lowpass filter prototype frequency responses.

Note that the range over n in the last equation is limited to $M/2 - 1$ due to the symmetry of $h[n]$ as suggested by (4). Although there are many solutions to the above equations, the half-sine windowing function [19],

$$h[n] = -\sin\left[\left(n + \frac{1}{2}\right)\frac{\pi}{2M}\right],$$

is used exclusively throughout this work as the MLT lowpass filter prototype. This windowing function is commonly used since it satisfies both the polyphase normalization, ensuring efficient implementation, and the perfect reconstruction criteria. Figure 2 illustrates the frequency response associated with the half-sine windowing function for $M = 64$. Whereas non-windowed FFT basis vectors yield sidelobes that are roughly 13 dB down from the main lobe, the level of attenuation in the sidelobes associated with the MLT basis vectors is approximately 23.5 dB.

With $K = 1$, the $M \times 2M$ transformation matrix, $\mathbf{\Psi}$, contains the LT basis set, $\{\psi_k[n], \ 0 \le k \le M-1, \ 0 \le n \le 2M-1\}$; thus there are M basis vectors with length $2M$. Transform domain signal processing using the MLT is illustrated in Figure 3. By segmenting the continuous input data stream, $x[n]$, into contiguous M-length data

7
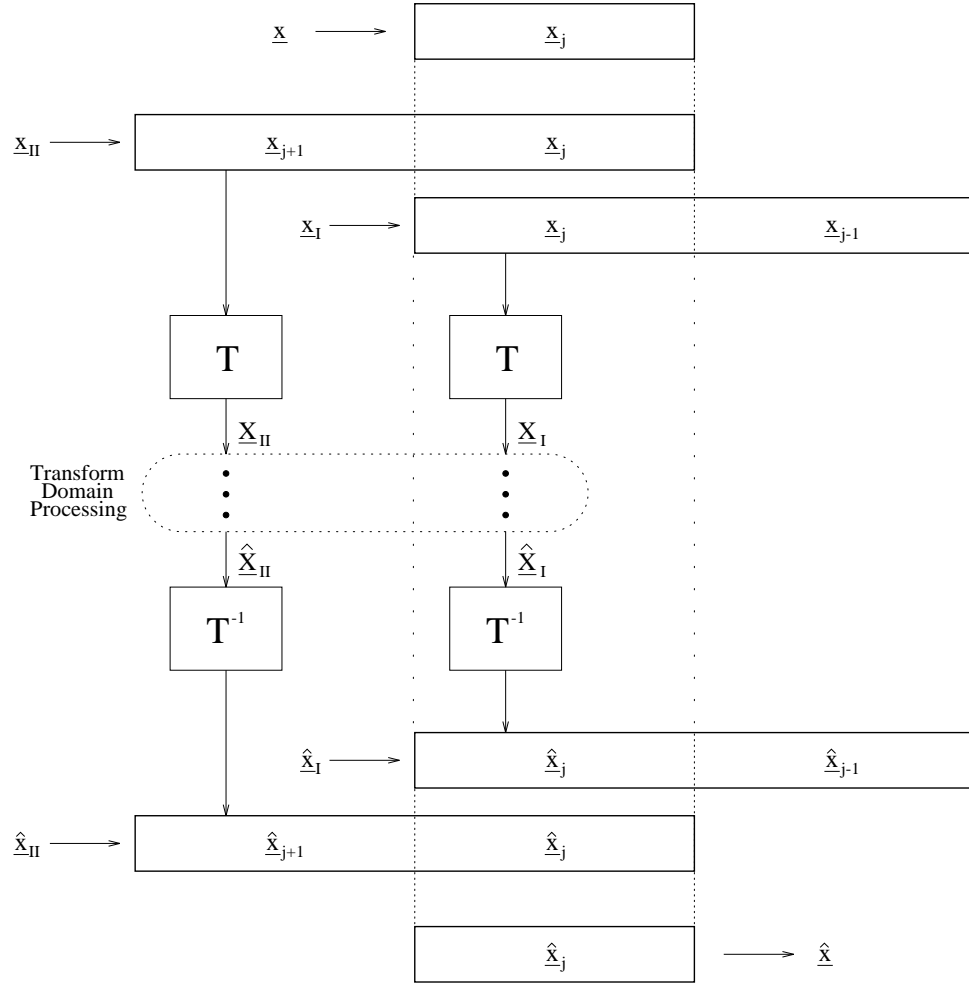
Figure 3: Signal processing using the MLT

blocks, successive data vectors, $\underline{x}_{j-1}$, $\underline{x}_j$ and $\underline{x}_{j+1}$ are defined as

$$
\underline{x}_l = \begin{bmatrix} x[lM] \\ x[lM+1] \\ \vdots \\ x[(l+1)M-1] \end{bmatrix} \qquad j-1 \le l \le j+1.
$$

Assuming that the data block of interest is the $M \times 1$ vector, $\underline{x}_j$, the LT analysis equations can be expressed in terms of the overlapping composite $2M \times 1$ input vectors,

$$
\underline{x}_I = \begin{bmatrix} \underline{x}_{j-1} \\ \hline \underline{x}_j \end{bmatrix} \qquad \text{and} \qquad \underline{x}_{II} = \begin{bmatrix} \underline{x}_j \\ \hline \underline{x}_{j+1} \end{bmatrix}
$$

as

$$
\underline{X}_I = \boldsymbol{\Psi}\underline{x}_I \tag{6}
$$

$$
\underline{X}_{II} = \boldsymbol{\Psi}\underline{x}_{II}. \tag{7}
$$

To obtain the original input vector, $\underline{x}_j$, from the above set of spectral coefficients, each of the overlapping input vectors must be reconstructed using the following synthesis, or inverse transform, expressions,

$$
\underline{\hat{x}}_I = \boldsymbol{\Psi}^T \underline{\hat{X}}_I
$$

$$
\underline{\hat{x}}_{II} = \boldsymbol{\Psi}^T \underline{\hat{X}}_{II},
$$

where

$$
\underline{\hat{x}}_I = \begin{bmatrix} \underline{\hat{x}}_{j-1} \\ \hline \underline{\hat{x}}_j \end{bmatrix} \qquad \text{and} \qquad \underline{\hat{x}}_{II} = \begin{bmatrix} \underline{\hat{x}}_j \\ \hline \underline{\hat{x}}_{j+1} \end{bmatrix}.
$$

Denoting the last M elements of $\underline{\hat{x}}_I$ and the first M elements of $\underline{\hat{x}}_{II}$ as $\underline{\hat{x}}_{j,I}$ and $\underline{\hat{x}}_{j,II}$, respectively, $\underline{\hat{x}}_j$ can be reconstructed from the above vectors as

$$
\underline{\hat{x}}_j = \underline{\hat{x}}_{j,I} + \underline{\hat{x}}_{j,II}
$$

or, equivalently, as

$$
\underline{\hat{x}}_j = \boldsymbol{\Psi}_I^T \underline{\hat{X}}_I + \boldsymbol{\Psi}_{II}^T \underline{\hat{X}}_{II}, \tag{8}
$$

9

where $\boldsymbol{\Psi}_{II}$ and $\boldsymbol{\Psi}_{I}$ denote the left and right $M \times M$ partitions of $\boldsymbol{\Psi}$, i.e.

$$\boldsymbol{\Psi} = [\boldsymbol{\Psi}_{II} \,|\, \boldsymbol{\Psi}_{I}].\tag{9}$$

2.1.3 Extended Lapped Transforms

As considered in this work, the ELT represents a subclass of lapped transforms with $K = 2$ and sinusoidally modulated basis vectors. As was the case with the MLT, the ELT basis vectors are generated by shifting the lowpass filter prototype, again denoted as $h[n]$, in the frequency domain such that the resulting M subband filters span the range of frequencies from zero to π. With an overlapping factor of 2, the length of the subband filters and, hence, $h[n]$, is four times the number of subbands. By allowing the time-support of the basis vectors to be spread over four data blocks, (3), after modifying the range of n such that $0 \leq n \leq 4M - 1$, can be used to define the sinusoidally modulated subband filters.

Whereas (4) and (5) were used in the previous section to represent the conditions placed on the MLT lowpass filter prototype by the PR constraints of (2), similar constraints for the ELT lowpass prototype can be expressed as [18]

$$h[4M - 1 - n] = h[n]\tag{10}$$

$$h^2[n] + h^2[n + M] + h^2[n + 2M] + h^2[n + 3M] = 1$$

$$h[n]h[n + 2M] + h[n + M]h[n + 3M] = 0$$

with $0 \leq n \leq 2M - 1$ in (10) and $0 \leq n \leq M/2 - 1$ in the last two equations. A class

of windows satisfying the above equations can be defined as [18]

$$h[\tfrac{M}{2} - 1 - i] \;\; = \;\; -\sin\theta_i \sin\theta_{M-1-i}$$

$$h[\tfrac{M}{2} + i] \;\; = \;\; \sin\theta_i \cos\theta_{M-1-i}$$

$$h[\tfrac{3M}{2} - 1 - i] \;\; = \;\; \cos\theta_i \sin\theta_{M-1-i}$$

$$h[\tfrac{3M}{2} + i] \;\; = \;\; \cos\theta_i \cos\theta_{M-1-i}$$

where $0 \leq i \leq M/2 - 1$ and the set of angles, θ_i, is given by

$$\theta_i = \left[\left(\frac{1-\gamma}{2M}\right)(2i+1) + \gamma\right]\frac{(2i+1)\pi}{8M}.$$

The additional parameter, γ, is a variable in the range $[0, 1]$ that controls the roll-off of the prototype frequency response. Consequently, γ controls the trade-off between stopband attenuation and transition bandwidth of $h[n]$ and, thus, the ELT basis vectors [19].

Figure 2 demonstrates the effect of different γ on $h[n]$ - note that for clarity the frequency responses of the lowpass filter prototypes are plotted only on the range $[0, 1/32]$ instead of $[0, 0.5]$. Clearly, maximum attenuation is achieved as γ approaches zero, whereas the bandwidth is minimized as it heads towards unity. Depending on the value of γ, the level of sidelobe attenuation may be anywhere from 22–34 dB.

For both simplicity and convenience, only ELT basis vectors derived from the above equations are considered in this work. For completeness, however, it should be noted that several techniques by which to develop optimal prototype filters have been presented in the literature [14, 33, 37]. A particularly appealing approach introduced by Vaidyanathan and Nguyen [33, 34, 44] utilizes eigenfilter design techniques to minimize the quadratic error in the passband and stopband of the prototype filter, $h[n]$. The resulting subband filters typically have very high attenuation in the stopbands and, thus, are characterized by low levels of inter-subband aliasing. Using

the eigenfilter approach, lowpass filter prototypes can also be designed with complex coefficients [34].

Whereas MLT $(K = 1)$ domain processing involves the use of three distinct data blocks, the ELT requires that seven different data segments, $\{\underline{x}_{j-3}, \underline{x}_{j-2}, \underline{x}_{j-1}, \underline{x}_j, \underline{x}_{j+1}, \underline{x}_{j+2}, \underline{x}_{j+3}\}$, be considered, where

$$\underline{x}_l = \begin{bmatrix} x[lM] \\ x[lM+1] \\ \vdots \\ x[(l+1)M-1] \end{bmatrix} \qquad j - 3 \leq l \leq j + 3.$$

Using these vectors, augmented $4M \times 1$ input vectors can be constructed as

$$\underline{x}_I = \begin{bmatrix} \underline{x}_{j-3} \\ \underline{x}_{j-2} \\ \underline{x}_{j-1} \\ \underline{x}_j \end{bmatrix} \qquad \underline{x}_{II} = \begin{bmatrix} \underline{x}_{j-2} \\ \underline{x}_{j-1} \\ \underline{x}_j \\ \underline{x}_{j+1} \end{bmatrix} \qquad \underline{x}_{III} = \begin{bmatrix} \underline{x}_{j-1} \\ \underline{x}_j \\ \underline{x}_{j+1} \\ \underline{x}_{j+2} \end{bmatrix} \qquad \underline{x}_{IV} = \begin{bmatrix} \underline{x}_j \\ \underline{x}_{j+1} \\ \underline{x}_{j+2} \\ \underline{x}_{j+3} \end{bmatrix}.$$

The corresponding analysis and synthesis equations thus become

$$
\begin{array}{ccc}
\text{Analysis Equations} & \Longleftrightarrow & \text{Synthesis Equations} \\
\underline{X}_I = \mathbf{\Psi}\underline{x}_I & & \hat{\underline{x}}_I = \mathbf{\Psi}^T \hat{\underline{X}}_I \\
\underline{X}_{II} = \mathbf{\Psi}\underline{x}_{II} & & \hat{\underline{x}}_{II} = \mathbf{\Psi}^T \hat{\underline{X}}_{II} \\
\underline{X}_{III} = \mathbf{\Psi}\underline{x}_{III} & & \hat{\underline{x}}_{III} = \mathbf{\Psi}^T \hat{\underline{X}}_{III} \\
\underline{X}_{IV} = \mathbf{\Psi}\underline{x}_{IV} & & \hat{\underline{x}}_{IV} = \mathbf{\Psi}^T \hat{\underline{X}}_{IV}.
\end{array}
$$

As in (8), partitioning the $M \times 4M$ ELT transformation matrix as

$$\mathbf{\Psi} = [\mathbf{\Psi}_{IV} \,|\, \mathbf{\Psi}_{III} \,|\, \mathbf{\Psi}_{II} \,|\, \mathbf{\Psi}_I],$$

allows the filtered data vector to be reconstructed from its ELT spectral representations as

$$\hat{\underline{x}}_j = \mathbf{\Psi}_I^T \hat{\underline{X}}_I + \mathbf{\Psi}_{II}^T \hat{\underline{X}}_{II} + \mathbf{\Psi}_{III}^T \hat{\underline{X}}_{III} + \mathbf{\Psi}_{IV}^T \hat{\underline{X}}_{IV}. \tag{11}$$

One can obtain a physical description of an ELT domain signal processing system by simply extending the MLT-based system shown in Figure 3 with two additional stages[22].

As considered in this work, the ELT represents a subclass of lapped transforms with $K = 2$. As was the case with the MLT, the ELT basis vectors are generated by shifting the lowpass filter prototype, again denoted as $h[n]$, in the frequency domain such that the resulting M subband filters span the range of frequencies from zero to 0.5π. With an overlapping factor of 2, the length of the subband filters and, hence, $h[n]$, is four times the number of subbands. By allowing the time-support of the basis vectors to be spread over four data blocks, viz. $0 \leq n \leq 4M - 1$, (3) can be used to define the sinusoidally modulated subband filters. As before, the selection and design of appropriate lowpass filter prototypes is not discussed here. In keeping with the discussion in [17, Section 5.2], the analysis and subsequent results presented herein assume that the chosen ELT lowpass prototype is designed with $\gamma = 0.5$.

Whereas MLT ($K = 1$) domain processing involves the use of three distinct data blocks, the ELT requires that seven different data segments, $\{\underline{x}_{j-3}, \underline{x}_{j-2}, \underline{x}_{j-1}, \underline{x}_j, \underline{x}_{j+1}, \underline{x}_{j+2}, \underline{x}_{j+3}\}$, be considered, where

$$
\underline{x}_l = \begin{bmatrix} x[lM] \\ x[lM + 1] \\ \vdots \\ x[(l+1)M - 1] \end{bmatrix} \qquad j - 3 \leq l \leq j + 3.
$$

Using these vectors, augmented $4M \times 1$ input vectors can be constructed as

$$
\underline{x}_I = \begin{bmatrix} \underline{x}_{j-3} \\ \underline{x}_{j-2} \\ \underline{x}_{j-1} \\ \underline{x}_j \end{bmatrix} \qquad \underline{x}_{II} = \begin{bmatrix} \underline{x}_{j-2} \\ \underline{x}_{j-1} \\ \underline{x}_j \\ \underline{x}_{j+1} \end{bmatrix} \qquad \underline{x}_{III} = \begin{bmatrix} \underline{x}_{j-1} \\ \underline{x}_j \\ \underline{x}_{j+1} \\ \underline{x}_{j+2} \end{bmatrix} \qquad \underline{x}_{IV} = \begin{bmatrix} \underline{x}_j \\ \underline{x}_{j+1} \\ \underline{x}_{j+2} \\ \underline{x}_{j+3} \end{bmatrix}.
$$

The corresponding analysis and synthesis equations thus become

$$
\underline{X}_{\mathcal{I}} = \mathbf{\Psi} \underline{x}_{\mathcal{I}} \qquad \text{and} \qquad \hat{\underline{x}}_{\mathcal{I}} = \mathbf{\Psi}^T \hat{\underline{X}}_{\mathcal{I}}, \tag{12}
$$

respectively, where $\mathcal{I} \in \{I, II, III, IV\}$.

As in (8), partitioning the $M \times 4M$ ELT transformation matrix as

$$
\mathbf{\Psi} = [\mathbf{\Psi}_{IV} \,|\, \mathbf{\Psi}_{III} \,|\, \mathbf{\Psi}_{II} \,|\, \mathbf{\Psi}_I]
$$

13
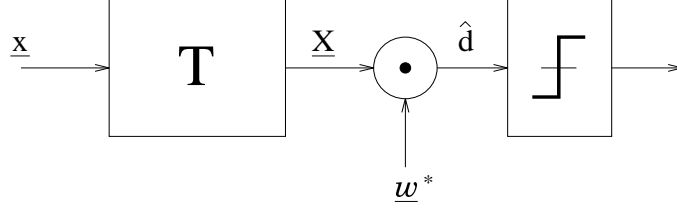
Figure 4: Receiver employing pre-correlation transform domain Wiener filtering.

allows the filtered data vector to be reconstructed from its ELT spectral representations as

$$\hat{\underline{x}}_j = \sum_{\mathcal{I}} \boldsymbol{\Psi}_{\mathcal{I}}^T \hat{\underline{X}}_{\mathcal{I}}. \tag{13}$$

One can obtain a physical description of an ELT domain signal processing system by simply extending the MLT-based system shown in Figure 3 with two additional stages [26].

2.2 Transform Domain Wiener Filtering

As illustrated in Figure 1, transform domain filtering offers a means of directly manipulating the spectral coefficients of the received data vector in an effort to suppress undesired interference. When the received data vectors are time-aligned with the data bits, i.e. each data block contains one complete data bit, detection may be performed directly in the transform domain. Under this condition and assuming that synchronization has been obtained, the inverse transform and correlation operation of Figure 1 may be replaced with a single dot product as shown in Figure 4. Here, $\underline{\alpha}$ has been replaced by the appropriate, possibly complex, set of Wiener filter coefficients, $\underline{w}^*$; $\underline{w}$ when the coefficients are strictly real. Note that if the identity transform is used and the Wiener filter is approximated using the LMS algorithm, this receiver reduces to the adaptive correlator receiver [35].

As an alternative to the pre-correlation receiver structure of Figure 4, one can equivalently use the receiver shown in Figure 5, which is called a "post-correlation"
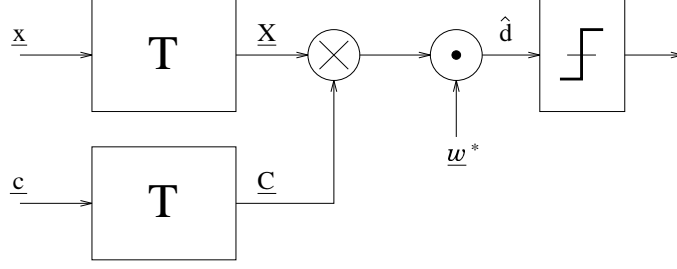
Figure 5: Receiver employing post-correlation transform domain Wiener filtering.

receiver due to the fact that the transform domain weighting function follows the correlator. In this receiver, the input signal, $x[n]$, and the reference spreading sequence are both processed by forward transforms and the results are multiplied point-by-point to perform the despreading operation. The point-wise products are then weighted by the adjustable taps and summed in order to generate the decision variable, $\hat{d}[n]$.

Pre- and post-correlation receivers yield identical BER results when their respective Wiener filter coefficients are utilized. As a result, the remainder of this work only considers the pre-correlation receiver structure where the despreading and interference suppression are performed with a single set of weights as in Figure 4. The following analysis and subsequent results can easily be rederived for the post-correlation receiver [22].

2.2.1 Block Transforms

The set of transform domain coefficients corresponding to the nth input data vector can be obtained using (1). The dot product of these coefficients and the complex conjugate of the weights, $\underline{w}^*$, produces an estimate of the transmitted data bit,

$$\hat{d}[n] = \underline{X}^T \underline{w}^*,$$

with the associated error signal defined as

$$\epsilon[n] \triangleq d[n] - \hat{d}[n], \tag{14}$$

15

where $d[n]$ is the transmitted data bit. Assuming that the desired signal energy is normalized to unity and that antipodal signaling is used, the corresponding MSE is given by

$$\mathcal{J}(\underline{w}) = E\left\{\epsilon[n]\epsilon^*[n]\right\} = 1 - \underline{w}^T\underline{k}_{d\underline{X}}^* - \underline{k}_{d\underline{X}}^T\underline{w}^* + \underline{w}^\dagger\mathbf{K}_{\underline{X}\underline{X}}\underline{w}, \tag{15}$$

where

$$\underline{k}_{d\underline{X}}^* = E\left\{d[n]\underline{X}^*\right\} \quad \text{and} \quad \underline{k}_{d\underline{X}}^T = E\left\{d^*[n]\underline{X}^T\right\}$$

define the cross-correlation between the transform of the input vector and desired signal and

$$\mathbf{K}_{\underline{X}\underline{X}} = E\left\{\underline{X}\underline{X}^\dagger\right\}$$

denotes the transform domain covariance matrix.

Setting the derivatives of $\mathcal{J}(\underline{w})$ with respect to the weighting vector to zero and solving yields the optimal transform domain Wiener filter coefficients,

$$\underline{w}_{pre} = \mathbf{K}_{\underline{X}\underline{X}}^{-1}\underline{k}_{d\underline{X}}.$$

Inserting $\underline{w}_{pre}$ into (15) yields the transform domain minimum MSE,

$$\mathcal{J}_{min} = 1 - \underline{w}_{pre}^T\underline{k}_{d\underline{X}}^* - \underline{k}_{d\underline{X}}^T\underline{w}_{pre}^* + \underline{w}_{pre}^\dagger\mathbf{K}_{\underline{X}\underline{X}}\underline{w}_{pre},$$

which upon simplification can be rewritten as

$$\mathcal{J}_{min} = 1 - \underline{k}_{d\underline{X}}^\dagger\mathbf{K}_{\underline{X}\underline{X}}^{-1}\underline{k}_{d\underline{X}}.$$

Assuming that the input data vector contains the spread data bit and zero-mean noise and interference, the expected value of the cross-correlation between its transform domain coefficients and those of the desired signal can be written as

$$\underline{k}_{d\underline{X}} = E\left\{d[n]\underline{X}\right\} = \underline{C},$$

where $\underline{C}$ represents the transform domain coefficients corresponding to the pseudo-noise spreading code, $\underline{c}$. Under these conditions, the minimum MSE is given by

$$\mathcal{J}_{min} = 1 - \underline{c}^{\dagger}\mathbf{K}_{\underline{xx}}^{-1}\underline{c}, \tag{16}$$

where $\mathbf{K}_{\underline{xx}}$ is the time domain covariance matrix.

2.2.2 Modulated Lapped Transforms

For the MLT, it is assumed that the number of filter bank subbands, M, is equal to the length, N, of the spreading sequence and, hence, the input data vector, $\underline{x}$, and that the length of each subband filter is $2M = 2N$. In the following analysis, it is also assumed that successive data bits are independent and that the power of the desired signal is normalized to unity. Only real signals and transforms are considered.

Since the MLT operates on overlapping data segments whose total lengths are the same as those of the subband filters, two sets of transform domain coefficients must be generated per data bit. Data bits modulated by the spreading code, $\underline{c}$, thus have their energy distributed among these sets of coefficients as

$$d^2[n] = 1 = \underline{c}^T\underline{c} = \underline{C}_I^T\underline{C}_I + \underline{C}_{II}^T\underline{C}_{II},$$

where

$$\underline{C}_{\mathcal{I}} = \mathbf{\Psi}\underline{c}_{\mathcal{I}}, \qquad \mathcal{I} \in \{I, II\} \tag{17}$$

and the time domain composite vectors, $\underline{c}_{\mathcal{I}}$, are given as

$$\underline{c}_I = \left[\begin{array}{c} \underline{0} \\ \hline \underline{c} \end{array}\right] \quad \text{and} \quad \underline{c}_{II} = \left[\begin{array}{c} \underline{c} \\ \hline \underline{0} \end{array}\right];$$

$\underline{0}$ denotes the $N \times 1$ zero vector. By partitioning the $N \times 2N$ transformation matrix as in (9), (17) can be rewritten as

$$\underline{C}_{\mathcal{I}} = \mathbf{\Psi}_{\mathcal{I}}\underline{c}.$$

17
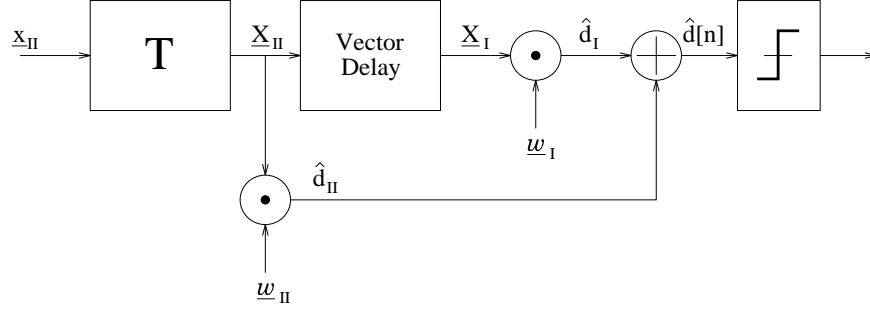
Figure 6: Receiver structure using pre-correlation MLT domain Wiener filtering.

Using both sets of transform domain coefficients, the original spreading sequence can be reconstructed as

$$\underline{c} = \mathbf{\Psi}_I^T \underline{C}_I + \mathbf{\Psi}_{II}^T \underline{C}_{II}. \tag{18}$$

Focusing on the received data block $\underline{x}_n$, as in Section 2.1.2, (6) and (7) establish the necessary expressions for the transform domain coefficients, $\underline{X}_I$ and $\underline{X}_{II}$, associated with each input vector. MLT domain filtering using the appropriate sets of tap weights, denoted as $\underline{w}_I$ and $\underline{w}_{II}$, produces the following estimates of the transmitted data bit,

$$\hat{d}_I[n] = \underline{X}_I^T \underline{w}_I \qquad \text{and} \qquad \hat{d}_{II}[n] = \underline{X}_{II}^T \underline{w}_{II},$$

which, when combined, yield the total estimate,

$$\hat{d}[n] = \hat{d}_I[n] + \hat{d}_{II}[n]. \tag{19}$$

Note that data block $\underline{x}_n$ is assumed to contain the actual data bit, $d[n]$. In practice, this process can be implemented using a pre-correlation MLT domain receiver like the one shown in Figure 6.

Given the definitions above, the total error between the estimate and the original data bit, as written in (14), is defined as

$$\epsilon[n] \triangleq d[n] - \underline{X}_I^T \underline{w}_I - \underline{X}_{II}^T \underline{w}_{II}.$$

18

Following the analysis used for block transforms, the corresponding MSE is given by

$$
\begin{aligned}
\mathcal{J}\left(\underline{w}_I, \underline{w}_{II}\right) \;=\;\; & 1 - 2\underline{k}_{d\underline{X}_I}\underline{w}_I - 2\underline{k}_{d\underline{X}_{II}}\underline{w}_{II} + \underline{w}_I^T \mathbf{K}_{\underline{X}\underline{X}}\underline{w}_I \\
& + 2\underline{w}_I^T \mathbf{K}_{\underline{X}_I\underline{X}_{II}}\underline{w}_{II} + \underline{w}_{II}^T \mathbf{K}_{\underline{X}\underline{X}}\underline{w}_{II},
\end{aligned}
\tag{20}
$$

where the cross-correlation vectors,

$$
\underline{k}_{d\underline{X}_{\mathcal{I}}} = E\left\{d[n]\underline{X}_{\mathcal{I}}\right\},
$$

the autocovariance matrices,

$$
\mathbf{K}_{\underline{X}\underline{X}} = \mathbf{K}_{\underline{X}_I\underline{X}_I} = \mathbf{K}_{\underline{X}_{II}\underline{X}_{II}} = E\left\{\underline{X}_I\underline{X}_I^T\right\}
$$

and the cross-covariance matrix $\mathbf{K}_{\underline{X}_I\underline{X}_{II}}$,

$$
\mathbf{K}_{\underline{X}_I\underline{X}_{II}} = E\left\{\underline{X}_I\underline{X}_{II}^T\right\},
$$

are evaluated in terms of the transform domain coefficients. Setting the partial derivatives of (20) with respect to $\underline{w}_I$ and $\underline{w}_{II}$ to zero, one obtains the following expressions for the MLT domain Wiener filter coefficients,

$$
\underline{w}_{pre_I} = \mathbf{K}_{\underline{X}\underline{X}}^{-1}\left(\underline{k}_{d\underline{X}_I} - \mathbf{K}_{\underline{X}_I\underline{X}_{II}}\underline{w}_{II}\right)
\tag{21}
$$

and

$$
\underline{w}_{pre_{II}} = \mathbf{K}_{\underline{X}\underline{X}}^{-1}\left(\underline{k}_{d\underline{X}_{II}} - \mathbf{K}_{\underline{X}_{II}\underline{X}_I}\underline{w}_I\right).
\tag{22}
$$

Simple substitution of $\underline{w}_{pre_{II}}$ for $\underline{w}_{II}$ in (21) yields

$$
\underline{w}_{pre_I} \;=\; \frac{\mathbf{K}_{\underline{X}\underline{X}}^{-1}\underline{k}_{d\underline{X}_I} - \mathbf{K}_{\underline{X}\underline{X}}^{-1}\mathbf{K}_{\underline{X}_I\underline{X}_{II}}\mathbf{K}_{\underline{X}\underline{X}}^{-1}\underline{k}_{d\underline{X}_{II}}}{\mathbf{I}_{N\times N} - \mathbf{K}_{\underline{X}\underline{X}}^{-1}\mathbf{K}_{\underline{X}_I\underline{X}_{II}}\mathbf{K}_{\underline{X}\underline{X}}^{-1}\mathbf{K}_{\underline{X}_{II}\underline{X}_I}}.
\tag{23}
$$

(22) can likewise be rewritten as

$$
\underline{w}_{pre_{II}} \;=\; \frac{\mathbf{K}_{\underline{X}\underline{X}}^{-1}\underline{k}_{d\underline{X}_{II}} - \mathbf{K}_{\underline{X}\underline{X}}^{-1}\mathbf{K}_{\underline{X}_{II}\underline{X}_I}\mathbf{K}_{\underline{X}\underline{X}}^{-1}\underline{k}_{d\underline{X}_I}}{\mathbf{I}_{N\times N} - \mathbf{K}_{\underline{X}\underline{X}}^{-1}\mathbf{K}_{\underline{X}_{II}\underline{X}_I}\mathbf{K}_{\underline{X}\underline{X}}^{-1}\mathbf{K}_{\underline{X}_I\underline{X}_{II}}}.
\tag{24}
$$

19

Assuming that successive data blocks are independent, expansion of the cross-covariance matrices yields

$$\mathbf{K}_{\underline{X}_I\underline{X}_{II}} = E\left\{\underline{X}_I\underline{X}_{II}^T\right\} = \mathbf{\Psi}_I\mathbf{K}_{\underline{xx}}\mathbf{\Psi}_{II}^T$$

and

$$\mathbf{K}_{\underline{X}_{II}\underline{X}_I} = \mathbf{\Psi}_{II}\mathbf{K}_{\underline{xx}}\mathbf{\Psi}_I^T.$$

(23) and (24) can thus be rewritten as

$$\underline{w}_{pre_I} = \frac{\mathbf{K}_{\underline{XX}}^{-1}\mathbf{k}_{d\underline{X}_I} - \mathbf{K}_{\underline{XX}}^{-1}\mathbf{\Psi}_I\mathbf{K}_{\underline{xx}}\mathbf{\Psi}_{II}^T\mathbf{K}_{\underline{XX}}^{-1}\mathbf{k}_{d\underline{X}_{II}}}{\mathbf{I}_{N\times N} - \mathbf{K}_{\underline{XX}}^{-1}\mathbf{\Psi}_I\mathbf{K}_{\underline{xx}}\mathbf{\Psi}_{II}^T\mathbf{K}_{\underline{XX}}^{-1}\mathbf{\Psi}_{II}\mathbf{K}_{\underline{xx}}\mathbf{\Psi}_I^T}$$

and

$$\underline{w}_{pre_{II}} = \frac{\mathbf{K}_{\underline{XX}}^{-1}\mathbf{k}_{d\underline{X}_{II}} - \mathbf{K}_{\underline{XX}}^{-1}\mathbf{\Psi}_{II}\mathbf{K}_{\underline{xx}}\mathbf{\Psi}_I^T\mathbf{K}_{\underline{XX}}^{-1}\mathbf{k}_{d\underline{X}_I}}{\mathbf{I}_{N\times N} - \mathbf{K}_{\underline{XX}}^{-1}\mathbf{\Psi}_{II}\mathbf{K}_{\underline{xx}}\mathbf{\Psi}_I^T\mathbf{K}_{\underline{XX}}^{-1}\mathbf{\Psi}_I\mathbf{K}_{\underline{xx}}\mathbf{\Psi}_{II}^T}$$

with the corresponding minimum MSE given by

$$
\begin{aligned}
\mathcal{J}_{min} &= \mathcal{J}(\underline{w}_{pre_I}, \underline{w}_{pre_{II}}) \\
&= 1 - 2\underline{k}_{d\underline{X}_I}\underline{w}_{pre_I} - 2\underline{k}_{d\underline{X}_{II}}\underline{w}_{pre_{II}} + \underline{w}_{pre_I}^T\mathbf{K}_{\underline{XX}}\underline{w}_{pre_I} \\
&\quad + 2\underline{w}_{pre_I}^T\mathbf{K}_{\underline{X}_I\underline{X}_{II}}\underline{w}_{pre_{II}} + \underline{w}_{pre_{II}}^T\mathbf{K}_{\underline{XX}}\underline{w}_{pre_{II}}.
\end{aligned}
\tag{25}
$$

At this point, it is not necessary to fully expand the above expression in terms of the cross-correlation vectors and matrices since an additional assumption may be made. In fact, if it is further assumed that the set of transform domain coefficients, $\underline{X}_I$ and $\underline{X}_{II}$, are also independent, then the cross-covariance matrices can be set to zero. Under this assumption, (23) and (24) simply reduce to

$$\underline{w}_{pre_{\mathcal{I}}} = \mathbf{K}_{\underline{XX}}^{-1}\underline{k}_{d\underline{X}_{\mathcal{I}}}, \qquad \mathcal{I} \in \{I, II\}, \tag{26}$$

thus simplifying the expression for the MSE as

$$\mathcal{J}(\underline{w}_{pre_I}, \underline{w}_{pre_{II}}) = 1 - \sum_{\mathcal{I}} \underline{k}_{d\underline{X}_{\mathcal{I}}}^T\mathbf{K}_{\underline{XX}}^{-1}\underline{k}_{d\underline{X}_{\mathcal{I}}}. \tag{27}$$

Given the input vector consisting of the spread data bit plus zero-mean noise and interference,

$$\underline{k}_{d\underline{X}_{\mathcal{I}}} = \underline{C}_{\mathcal{I}}.$$

The corresponding Wiener filter coefficients are given by

$$\underline{w}_{pre_{\mathcal{I}}} = \mathbf{K}_{\underline{XX}}^{-1}\underline{C}_{\mathcal{I}}.$$

Consequently,

$$\mathcal{J}(\underline{w}_{pre_I}, \underline{w}_{pre_{II}}) = 1 - \sum_{\mathcal{I}} \underline{C}_{\mathcal{I}}^T \mathbf{K}_{\underline{XX}}^{-1} \underline{C}_{\mathcal{I}} \qquad (28)$$

represents the minimum MSE.

Clearly, with the assumption that $\underline{X}_I$ and $\underline{X}_{II}$ are independent, (26) does not represent the true set of transform domain Wiener filter coefficients. Hence, the MSE expressions presented in (27) and (28) do not represent the true minimum MSE. If exact solutions for the Wiener coefficients and, hence, the minimum MSE are required, $\underline{w}_{pre_I}$ and $\underline{w}_{pre_{II}}$ as given by (23) and (24) must be used in (25). Through both analytical and experimental evaluation, however, the difference between these two sets of expressions for $\underline{w}_{pre_I}$ and $\underline{w}_{pre_{II}}$ has been determined to be negligible for the input signals under consideration. Thus, without significantly compromising the analysis, the assumption of independence between the transform domain coefficients is maintained throughout this work.

2.2.3   Extended Lapped Transforms

The development of the Wiener coefficients for the ELT is directly analogous to that presented for the MLT [22] and, consequently, is not presented. The major difference when using the ELT is that four sets of transform domain coefficients must be computed for each input data bit instead of two. These additional weights result from the fact that the ELT processes overlapping data segments consisting of four

N-length input vectors as discussed in Section 2.1.3. As in the case of the MLT, the longer basis vectors associated with the ELT improve spectral resolution by increasing stopband attenuation in neighboring subbands. For narrow-band interference, such an improvement enhances excision performance and is expected to yield a high fidelity power spectral estimate for use in normalized transform domain LMS algorithms.

2.3 Bit Error Rate Analysis

Assuming that the receiver has knowledge of both carrier frequency and phase and that binary antipodal signaling is used, modem operations appear distortionless and yield real data signals; such a system is thus viewed as a coherent baseband BPSK communication system. Under these conditions, the generalized discrete-time transform domain filtering receiver shown in Figure 4 is analyzed.

With respect to Figure 4, the receiver input, $x[n]$, is assumed to consist of the sum of the transmitted signal, additive thermal noise and interference, i.e.

$$x[n] = \pm s[n] + \eta[n] + j[n].$$

Each data bit is modulated by an entire length-N PN sequence and sampled once per chip with the energy-per-bit, E_b, normalized to unity. Thus, each spread data bit may be expressed as

$$s[n] = d[n]c[n] \qquad n = 0, 1, \ldots, N - 1$$

where $d[n] \in \{+1, -1\}$ and $c[n] \in \{+\frac{1}{\sqrt{N}}, -\frac{1}{\sqrt{N}}\}$ represent the random binary data bit sequence and PN code samples, respectively. The thermal noise samples, $\eta[n]$, are assumed to be additive white Gaussian noise (AWGN) samples with two-sided power spectral density, $N_0/2$, and the interference samples are assumed to be generated from the single-tone interferer, $j[n] = A_j \cos[\delta\omega n + \theta]$, where A_j is a constant denoting amplitude, $\delta\omega$ is the offset from the carrier frequency and θ is a random phase uniformly distributed in the interval $[0, 2\pi)$. The received signal data samples
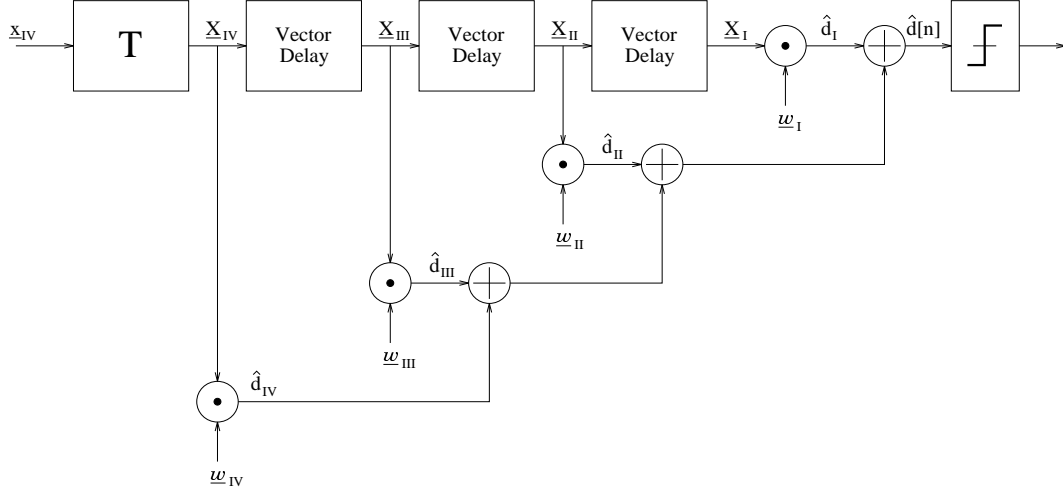
22

Figure 7: Receiver structure using pre-correlation ELT domain Wiener filtering.

are divided into disjoint sets corresponding to individual data bits and are processed and detected independently.

To facilitate further analysis, a $+1$ data bit is assumed to have been transmitted, i.e. $\underline{s} = \underline{c}$. Thus, in accordance with Figure 4, the bit decision variable, $\hat{d}$, for the block transform domain pre-correlation receiver can be expressed as

$$
\begin{aligned}
\hat{d} &= \underline{w}_{pre}^{\dagger} \underline{X} \\
&= \underline{w}_{pre}^{\dagger} \left(\underline{C} + \underline{N} + \underline{J} \right),
\end{aligned}
$$

where $\underline{C}$, $\underline{N}$ and $\underline{J}$ represent transforms of the input vectors $\underline{c}$, $\underline{\eta}$ and $\underline{j}$. In a similar manner, $\hat{d}$ associated with the pre-correlation receivers based on lapped transforms shown in Figures 6 and 7 is given by

$$
\begin{aligned}
\hat{d} &= \sum_{\mathcal{I}} \underline{w}_{pre_{\mathcal{I}}}^{\dagger} \underline{X}_{\mathcal{I}} \\
&= \sum_{\mathcal{I}} \underline{w}_{pre_{\mathcal{I}}}^{\dagger} \left(\underline{C}_{\mathcal{I}} + \underline{N}_{\mathcal{I}} + \underline{J}_{\mathcal{I}} \right),
\end{aligned}
$$

where $\mathcal{I} \in \{I, II\}$ for the MLT and $\mathcal{I} \in \{I, II, III, IV\}$ for the ELT.

Given that its polarity indicates the value of the transmitted data bit, $\hat{d}$ is put through a threshold device with the decision boundary set to zero to yield a bit

23

decision. By determining the first and second order statistics of $\hat{d}$, BER expressions can be derived and evaluated for arbitrary $\hat{x}[n]$. Since $\hat{x}[n]$ depends explicitly on the transform or filter bank used, the evaluation of these equations is equivalent to directly relating the receiver BER to the analysis/synthesis techniques employed.

Since the jammer phase, θ, is unknown, the conditional mean, $\mu_{\hat{d}|\theta}$ of $\hat{d}$ is first determined for a fixed value of θ. Assuming that the transform domain filter coefficients and transformation matrix are fixed, the conditional expectation of $\hat{d}$ may be expressed as

$$\mu_{\hat{d}|\theta} = \underline{w}_{pre}^{\dagger} \left(\underline{C} + \underline{J}_{\theta} \right),$$

where $\underline{J}_{\theta}$ emphasizes the conditioning on θ. Since the noise term is independent of the narrow-band interference, the variance of $\hat{d}$ is not a function of θ and can be written as

$$\sigma_{\hat{d}}^2 = \frac{N_0}{2} \sum_{k=0}^{N-1} |w_{pre,k}|^2.$$

When using lapped transforms, the conditional mean is given by

$$\mu_{\hat{d}|\theta} = \sum_{\mathcal{I}} \underline{w}_{pre_{\mathcal{I}}}^{T} \left(\underline{C}_{\mathcal{I}} + \underline{J}_{\mathcal{I},\theta} \right)$$

with the corresponding variance,

$$\sigma_{\hat{d}}^2 = \frac{N_0}{2} \sum_{k=0}^{N-1} \sum_{\mathcal{I}} w_{pre_{\mathcal{I}},k}^2.$$

Using these expressions for $\mu_{\hat{d}|\theta}$ and $\sigma_{\hat{d}}^2$, the BER performance of the various pre-correlation receivers can be evaluated for an arbitrary set of basis vectors and spreading codes. Assuming equiprobable data bits, the probability of bit error is given by

$$P_e = \frac{1}{2\pi} \int_0^{2\pi} Q \left(\frac{\mu_{\hat{d}|\theta}}{\sigma_{\hat{d}}} \right) d\theta,$$

where the Q-function is defined as

$$Q(k) \triangleq \frac{1}{\sqrt{2\pi}} \int_k^{\infty} e^{-t^2} dt.$$

2.4 Analytical and Simulated BER Results

In this section, the results of several computer simulations are used to illustrate the BER performance of the spread spectrum communications receivers depicted in Figures 4 and 5 and are compared to theoretical predictions based on the analysis of the previous section. In each case, a 64-chip augmented PN sequence is used to directly modulate a binary input data stream sampled at a rate of 64 samples per bit; simulations are performed at baseband at a normalized data rate of 1 Hz. The resulting spread data signal is transmitted over an AWGN channel with narrow-band interference and, at the receiver, non-windowed block (64×64) and lapped ($64 \times 128 \cdot K$) transforms map the received time domain waveform into the transform domain.

Since the presentation of Wiener filtering results by themselves offers little insight into the receiver's interference mitigation ability, Wiener-based performance is illustrated alongside that obtained via transform domain excision. As in [26], excision is performed using a fixed k-bin excision scheme in which the spectral weights corresponding to the bins with the largest average magnitude are set to zero; those remaining are set equal to unity. Given that excision performance is dependent on the number of transform domain bins excised, preliminary analyses and simulations have been performed to determine the optimal number of bins to excise in each case. The actual number of bins removed in each jamming scenario is shown in parentheses in the figure legends.

Figures 8 – 9 show BER results obtained using block transform (BT) domain excision and and Wiener weights in the presence of single-tone jammers with frequency offsets from the carrier, $\delta\omega$, of 0.117, 0.127 and 0.252, respectively, relative to a normalized chip rate of unity. Each jammer has a power level 20 dB above that of the signal, thus causing the BER performance to approach 0.5 when no suppression techniques are used. Since, as in (16), BT domain Wiener filtering performance is
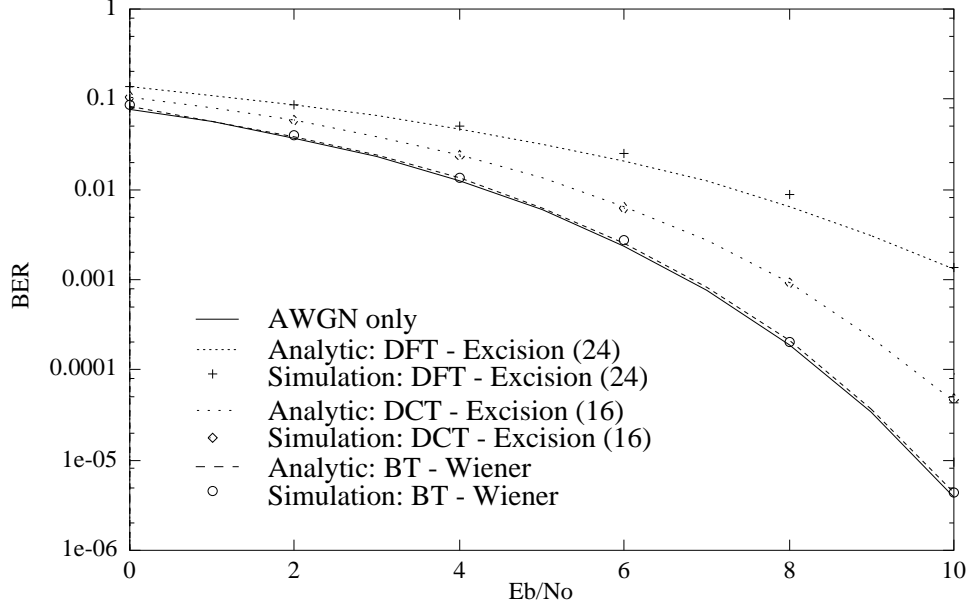
Figure 8: BER performance using excision and Wiener coefficients, $\delta\omega = 0.1171875$

independent of the underlying transform [22], both DCT and DFT-based Wiener filtering results are depicted by a single plot in each figure. From these figures, it is clear that Wiener filtering is less sensitive to jammer frequency and consistently yields BER performance within 0.25 dB of the theoretical performance in AWGN alone. In practice, however, such an approach typically necessitates the use of adaptive algorithms which require more time to converge.

In contrast to Wiener filtering, transform domain excision algorithms converge faster, thus making them more adept at suppressing rapidly time-varying interferers, and are typically easier to implement. As demonstrated in Figures 8 – 9, however, BER performance is dictated by how well the transform basis vectors match the interfering signal of interest. For best performance, excision requires that the interference energy be confined to a small number of transform domain bins as is the case for the DCT in Figure 9. Although in this case, the simple exciser performs as well as the Wiener filter, Figures 8 and 10 clearly show different scenarios in which the excision
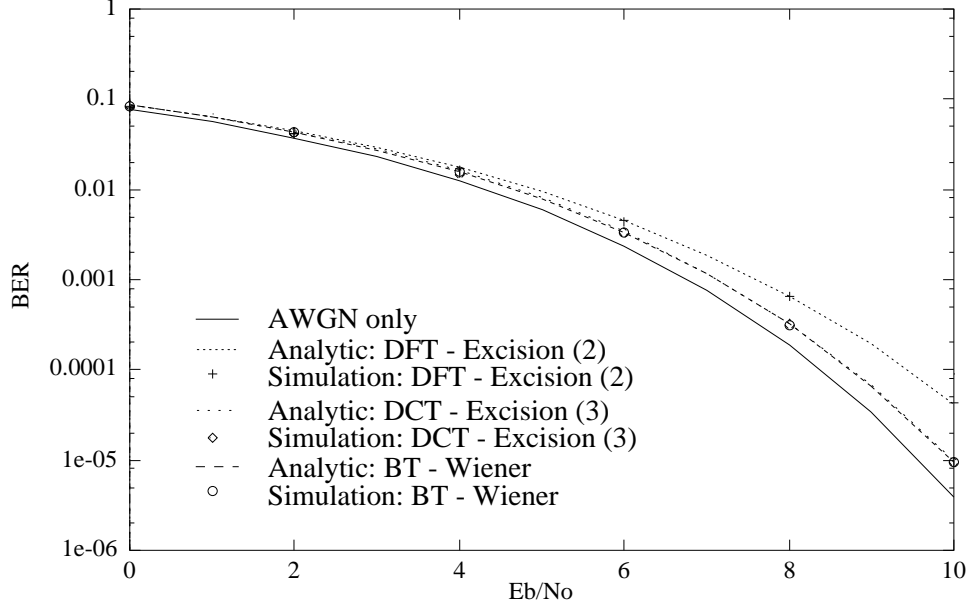
Figure 9: BER performance using excision and Wiener coefficients, $\delta\omega = 0.251953125$

algorithm may yield insufficient BER improvement. As in most engineering problems, a fundamental trade-off exists between Wiener filtering and excision; it is up to the user to decide whether BER performance or algorithmic convergence rates are more critical.

Figure 11 demonstrates the agreement in BER between the analytical expressions and simulation results obtained using lapped transform domain excision and Wiener filtering. Since MLT and ELT domain Wiener filter performances are virtually identical, only one set of results, labeled LT, are depicted. From this figure, it is clear that the disparity between the excision and Wiener filtering results is much less than that corresponding to the block transform implementation. Such a result suggests that narrow-band interference suppression via lapped transform domain excision may be used in lieu of Wiener filtering approaches using either block or lapped transforms. Despite this suggestion, however, Wiener filtering still displays a non-negligible level of additional improvement that is likely to be more robust with respect to jammer
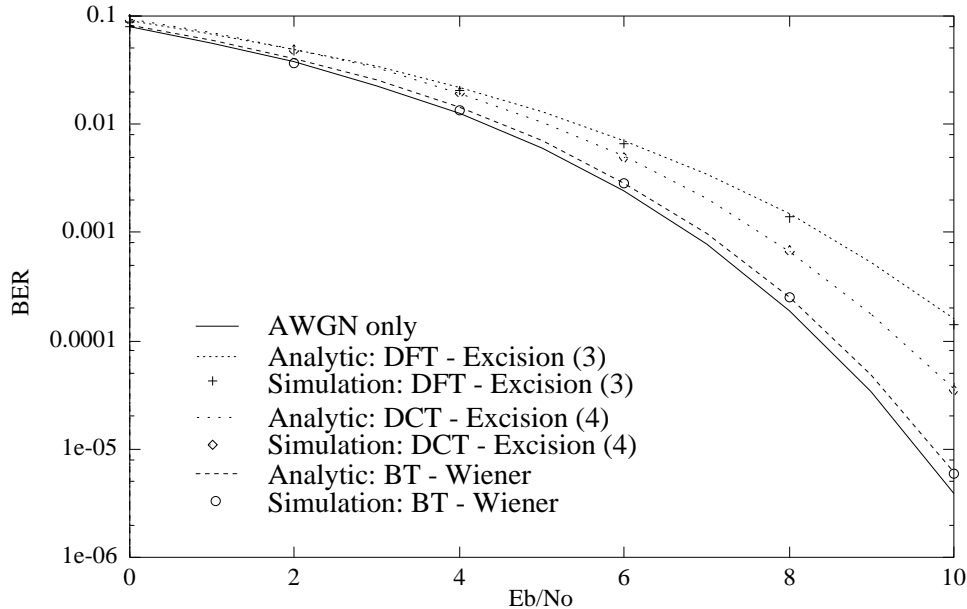
Figure 10: BER performance using excision and Wiener coefficients, $\delta\omega = 0.126984$

frequency and bandwidth. A more thorough comparison of these excision results with those illustrated in Figure 10 is presented in [26].

3   Nonlinear Filtering in the Transform Domain

Transform domain filtering using real-time Fourier transforms and surface acoustic wave (SAW) devices was originally proposed as a means to suppress narrow-band interference in continuous-time spread spectrum receivers [28]. In related works [6, 29, 39], it was further developed and extended to transform domain excision techniques based on the Fourier transform. Within the past few years, several authors have proposed the use of wavelet transforms and related filter banks as an alternative to the fast Fourier transform (FFT) [12, 24, 27, 36, 40, 41]. In one of the earliest applications, the efficient implementation of digital filter banks using polyphase structures was used to demonstrate the effectiveness of multirate filter banks in excising narrow-band interference [12]. It has since been shown that the data compression ability
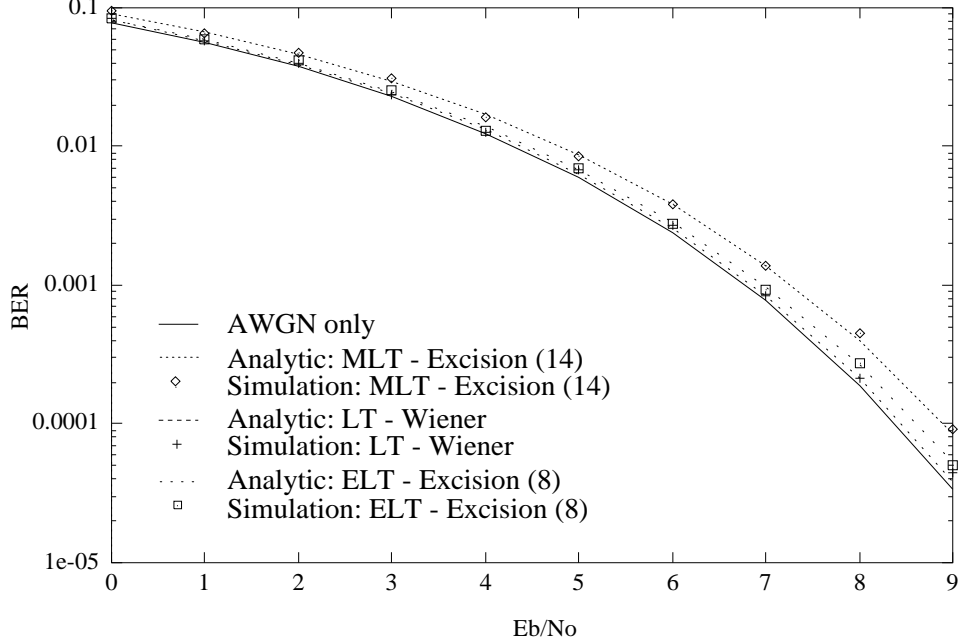
Figure 11: BER performance using lapped transform domain excision and Wiener filtering, JSR = 20 dB, $\delta\omega = 0.126984$ rad/sec.

associated with wavelet transforms can be used to compactly represent sinusoidal interferers using hierarchical subband trees [24, 27, 36, 43].

Most recently, excision using filter banks [22] and "spectrally-contained orthogonal transforms" (SCOT) [40, 41] has also been shown to be very effective at mitigating narrow-band interference. The analysis presented in [22] focuses on the development and analysis of transform domain filtering and data demodulation/detection schemes using orthonormal block and lapped transforms (LT) and forms the basis for this work. In a similar manner, the work presented in [40] essentially addresses the application of narrow-band excision using time-weighted discrete Fourier transforms (DFT) to data demodulation and closely examines its corresponding bit error rate (BER) performance. In contrast, the excision analysis offered in [41] focuses primarily on the use of time-weighted DFTs and cosine-modulated filter banks for radiometric signal detection. Whereas [40] and [41] independently address BER performance
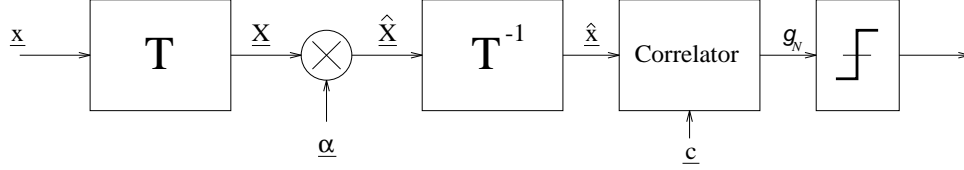
29

Figure 12: Discrete-time receiver employing transform domain filtering.

and the application of SCOTs, particularly cosine-modulated filter banks, to interference suppression, the primary goal of this work is to present a thorough analysis and evaluation of the lapped transform domain excision process as a means of mitigating narrow-band interference.

Transform domain excision is frequently performed using a receiver such as the one shown in Figure 12. Here, blocks $\mathbf{T}$ and $\mathbf{T}^{-1}$ represent arbitrary forward and inverse M-point transforms, respectively, and the transform domain weighting vector, $\underline{\alpha}$, is assumed to contain binary elements, i.e. $\{\alpha_k \in \{0, 1\}, \ 0 \leq k \leq M - 1\}$. The individual components of the binary weighting vector vary in response to the changes in the distribution of interference energy present in each received data vector — excision is a simple technique that suppresses narrow-band interference by setting portions of the transform that are primarily interference to zero. Due to its binary nature, the excision process typically yields poorer BER performance than more sophisticated transform domain Wiener filtering schemes [22] unless all of the interference energy is contained in a very small number of transform domain bins. Nevertheless, in many cases, the simplicity of the receiver structure and the ability of the exciser to react rapidly to changes in the interference make it a prime choice in many narrow-band interference suppression applications [1, 2, 5, 10, 23, 38].

As previously mentioned, this work further develops the excision process by considering the application of lapped transforms [19] in the transform domain exciser. With LTs, the basis vectors are not restricted in length as they are in conventional block transforms like the DFT and discrete cosine transform (DCT). Indeed, whereas

30

the lengths of the block transform basis vectors are limited to the number of transform domain cells, or bins, the LT basis vectors have length, L, that is equal to some even integer multiple of the number of bins, i.e. $L = 2KM$, where M is the number of bins and K is the *overlapping factor* [19]; the inputs to successive transforms are produced by overlapping segments of the received signal. Thus, in comparison to traditional length-M basis vectors, the basis vectors associated with LTs typically yield improved stopband attenuation in the frequency domain for a given filter bandwidth. Fortunately, there exist efficient filter bank structures that allow these longer basis vectors to be used while only moderately increasing the number of required arithmetic operations [19].

3.1 Transform Domain Excision and Detection

In this section, the bit error rate (BER) performance of lapped transform domain excisers in the presence of single-tone and narrow-band Gaussian interference is derived. Although not considered here, the extension of the BER analysis to multiple-tone interference is straightforward and is discussed in some detail in [31]. An expression for the BER is first derived using the MLT and then modified to yield a similar expression for ELT domain excision. The BER performance analysis for transform domain excision using orthonormal block transforms [24, 22] is not presented here; however, results for block transforms will be used for comparison in the next section. Throughout this section, modulation/demodulation operations between the transmitter and receiver are assumed to be transparent. Hence, the receiver is assumed to have perfect knowledge of the carrier frequency and phase and the corresponding received data signal is real. Antipodal signaling is used and each data bit is spread using one full length of the spreading sequence. Furthermore, the received signal is sampled once per chip, the length of the spreading sequence equals the number of transform bins, M, and the boundaries of the transform input vectors are aligned with those of

31

the data bit.

The received signal is assumed to consist of the sum of the transmitted signal, additive thermal noise and interference, i.e.

$$\underline{r} = \underline{s} + \underline{\eta} + \underline{j}.$$

Here, $\underline{s}$ represents the spread data bit,

$$\underline{s} = d[n]\underline{c},$$

where $d[n]$ is the current data bit with $d[n] \in \{+1, -1\}$ and $\underline{c}$ is the spreading code with chip values of $\pm\frac{1}{\sqrt{M}}$, and $\underline{\eta}$ is a vector of zero-mean white Gaussian noise (AWGN) samples with two-sided power spectral density $N_0/2$. Samples of the interference vector, $\underline{j}$, are assumed to be generated from the single-tone interferer, $j[n] = A_j \cos[\delta\omega n + \theta]$, where A_j is a constant denoting amplitude, $\delta\omega$ is the offset from the carrier frequency and θ is a random phase uniformly distributed in the interval $[0, 2\pi)$.

3.1.1 Modulated lapped transforms

Assuming synchronization, the current data block, denoted as $\underline{x}_j$ in Section 2.1.2, can be equivalently represented by the received data vector, i.e. $\underline{x}_j = \underline{r}$. As defined in Eqs. 6 and 7, the MLT domain coefficients corresponding to the received data vector, $\underline{r}$, are thus given as

$$\underline{R}_I = \mathbf{\Psi}\underline{r}_I$$
$$\underline{R}_{II} = \mathbf{\Psi}\underline{r}_{II}.$$

Since MLT domain processing necessitates the use of two sets of transform domain filter coefficients, denoted as $\underline{\alpha}_I$ and $\underline{\alpha}_{II}$, the modified spectral coefficients may be expressed as

$$\hat{\underline{R}}_I = \text{diag}(\underline{\alpha}_I)\underline{R}_I \quad \text{and} \quad \hat{\underline{R}}_{II} = \text{diag}(\underline{\alpha}_{II})\underline{R}_{II}. \tag{29}$$

Note that here diag $(\cdot)$ denotes the $M \times M$ matrix whose diagonal elements correspond to the components of its $M \times 1$ argument. Given Eq. 8, the $M \times 1$ filtered data vector may be written as

$$\hat{\underline{r}} = \sum_{\mathcal{I}} \mathbf{\Psi}_{\mathcal{I}}^T \hat{\underline{R}}_{\mathcal{I}}, \qquad \mathcal{I} \in \{I, II\}. \tag{30}$$

The filtered data vector can be correlated with the reference spreading code to yield the bit decision variable,

$$g_{N,MLT} = \underline{c}^T \hat{\underline{r}}.$$

With the additional assumption that the overall system is linear, $g_{N,MLT}$ may be rewritten in terms of the individual signal components using Eqs. 29 and 30 as [22]

$$
\begin{aligned}
g_{N,MLT} &= \sum_{\mathcal{I}} \underline{C}_{\mathcal{I}}^T \mathrm{diag}(\underline{\alpha}_{\mathcal{I}}) \underline{R}_{\mathcal{I}} \\
&= \sum_{\mathcal{I}} \underline{C}_{\mathcal{I}}^T \mathrm{diag}(\underline{\alpha}_{\mathcal{I}}) \left[\underline{S}_{\mathcal{I}} + \underline{N}_{\mathcal{I}} + \underline{J}_{\mathcal{I}} \right],
\end{aligned}
$$

where $\underline{C}_{\mathcal{I}} = \mathbf{\Psi}_{\mathcal{I}} \underline{c}$. $\underline{S}_{\mathcal{I}}$, $\underline{N}_{\mathcal{I}}$ and $\underline{J}_{\mathcal{I}}$ correspond to the transform domain representations of the desired signal, additive white Gaussian noise and interference components, respectively. This expression shows how detection can be performed in the transform domain, i.e. *without* performing an inverse transform. Figure 13 illustrates a generic communications receiver employing MLT domain excision and detection. In this system, the spectral coefficients of the observed data signal are point-wise multiplied with the weighting vector elements. The corresponding outputs are then correlated with the known transform domain reference vectors, using a dot product, to yield the decision variable.

In practice $g_{N,MLT}$ is typically put through a threshold device with the decision boundary set to zero to make a bit decision. By determining the first and second-order statistics of $g_{N,MLT}$, the conditional and unconditional bit error rate expressions can be evaluated for arbitrary input signals, spectral weights and linear transforms.
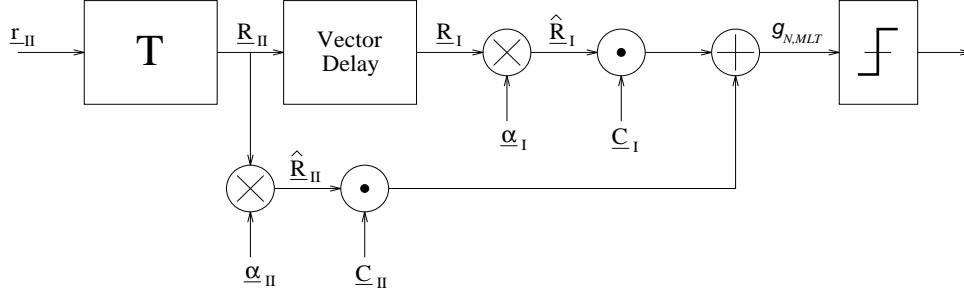
33

Figure 13: Receiver employing MLT domain excision and detection.

Since the jammer phase, θ, is unknown, the conditional mean, $\mu_{g,MLT|\theta}$, of $g_{N,MLT}$ must first be determined for a fixed value of θ. Assuming that the transform domain filter coefficients and transformation matrix are fixed and that a $+1$ data bit has been sent, i.e. $\underline{s} = \underline{c}$, the conditional expectation of $g_{N,MLT}$ may be expressed as

$$
\begin{aligned}
\mu_{g,MLT|\theta} &= E\left\{g_{N,MLT} \,|d[n] = +1, \theta\right\} \\
&= \sum_{\mathcal{I}} \underline{C}_{\mathcal{I}}^{T} \mathrm{diag}(\underline{\alpha}_{\mathcal{I}}) \left(\underline{C}_{\mathcal{I}} + \underline{J}_{\mathcal{I},\theta}\right),
\end{aligned}
\tag{31}
$$

where $\underline{J}_{\mathcal{I},\theta}$ is defined as

$$
\underline{J}_{\mathcal{I},\theta} = E\left\{\underline{J}_{\mathcal{I}} \,|\theta\right\}.
\tag{32}
$$

Clearly, if the weighting vector elements are set to unity, the receiver simply correlates the transforms of the received signal with those of the spreading code.

Assuming that the zero-mean noise terms are independent of the signal and interference components and that each set of transform domain coefficients is independent of the others, the conditional second-order moment of $g_{N,MLT}$ may be written as

$$
E\left\{g_{N,MLT}^{2} \,|d[n], \theta\right\} = \mu_{g,MLT|\theta}^{2} + \sum_{\mathcal{I}} \underline{C}_{\mathcal{I}}^{T} \mathrm{diag}(\underline{\alpha}_{\mathcal{I}}) \mathbf{K}_{\underline{N}_{\mathcal{I}}\underline{N}_{\mathcal{I}}} \mathrm{diag}(\underline{\alpha}_{\mathcal{I}}) \underline{C}_{\mathcal{I}},
$$

where

$$
\mathbf{K}_{\underline{N}_{\mathcal{I}}\underline{N}_{\mathcal{I}}} = E\left\{\underline{N}_{\mathcal{I}}\underline{N}_{\mathcal{I}}^{T}\right\} = \sigma_{\eta}^{2}\mathbf{I} = \frac{N_{0}}{2}\mathbf{I}.
$$

34

Thus, the variance of $g_{N,MLT}$ is given by

$$
\begin{aligned}
\sigma^2_{g,MLT|\theta} &= E\left\{g^2_{N,MLT} |d[n], \theta\right\} - \mu^2_{g,MLT|\theta} \\
&= \frac{N_0}{2} \sum_{\mathcal{I}} \underline{C}^T_{\mathcal{I}} \mathrm{diag}(\underline{\alpha}_{\mathcal{I}}) \mathrm{diag}(\underline{\alpha}_{\mathcal{I}}) \underline{C}_{\mathcal{I}}.
\end{aligned}
\tag{33}
$$

Clearly, since the dependence on θ has been removed, $\sigma^2_{g,MLT} = \sigma^2_{g,MLT|\theta}$.

Using the expressions for $\mu_{g,MLT|\theta}$ and $\sigma^2_{g,MLT}$, as given by Eqs. 31 and 33, one can evaluate the BER performance of the receiver depicted in Figure 13 for an arbitrary set of basis vectors and spreading code. Assuming equiprobable data bits, the probability of bit error is given by [22]

$$
P_{e,MLT} = \frac{1}{2\pi} \int_0^{2\pi} Q\left(\frac{\mu_{g,MLT|\theta}}{\sigma_{g,MLT}}\right) d\theta,
$$

where the Q-function is defined as

$$
Q(k) \triangleq \frac{1}{\sqrt{2\pi}} \int_k^\infty e^{-t^2} dt.
$$

3.1.2 Extended Lapped Transforms

Using Eq. 11 and denoting the four sets of transform domain filter coefficients as $\underline{\alpha}_I$, $\underline{\alpha}_{II}$, $\underline{\alpha}_{III}$ and $\underline{\alpha}_{IV}$, the ELT domain filtered input vector is written as

$$
\hat{\underline{r}} = \sum_{\mathcal{I}} \boldsymbol{\Psi}^T_{\mathcal{I}} \hat{\underline{R}}_{\mathcal{I}}, \quad \mathcal{I} \in \{I, II, III, IV\},
\tag{34}
$$

where the modified ELT domain coefficients are given by

$$
\hat{\underline{R}}_{\mathcal{I}} = \mathrm{diag}(\underline{\alpha}_{\mathcal{I}}) \underline{R}_{\mathcal{I}}.
\tag{35}
$$

Given Eqs. 34 and 35, the ELT domain decision variable can be expressed as

$$
\begin{aligned}
g_{N,ELT} &= \underline{c}^T \hat{\underline{r}} \\
&= \sum_{\mathcal{I}} \underline{C}^T_{\mathcal{I}} \mathrm{diag}(\underline{\alpha}_{\mathcal{I}}) \left[\underline{S}_{\mathcal{I}} + \underline{N}_{\mathcal{I}} + \underline{J}_{\mathcal{I}}\right].
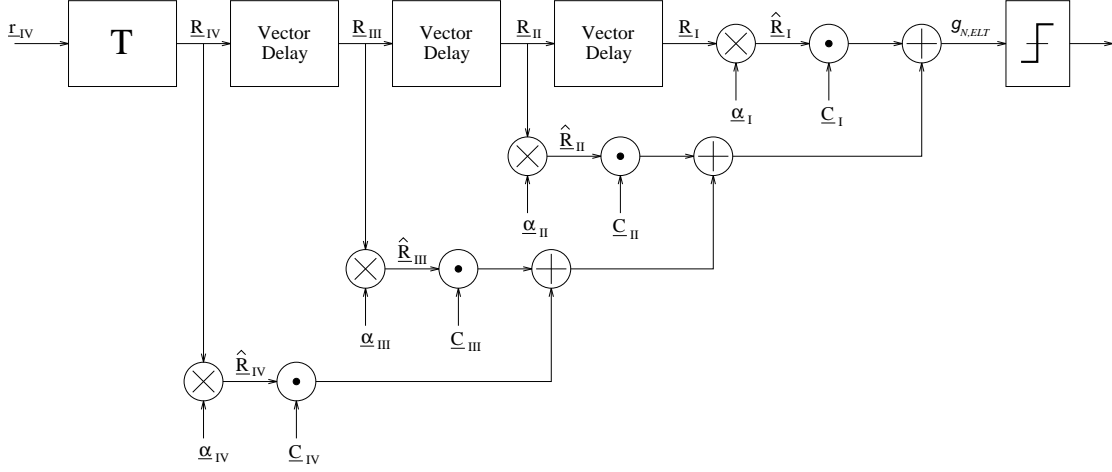\end{aligned}
$$

Figure 14: Receiver employing ELT domain excision and detection.

From this expression, the conditional mean of $g_{N,ELT}$ with respect to $d[n] = +1$ and θ is given by

$$\mu_{g,ELT|\theta} \;=\; \sum_{\mathcal{I}} \underline{C}_{\mathcal{I}}^{T} \mathrm{diag}(\underline{\alpha}_{\mathcal{I}}) \left(\underline{C}_{\mathcal{I}} + \underline{J}_{\mathcal{I},\theta} \right), \tag{36}$$

where the $\underline{J}_{\mathcal{I},\theta}$ terms follow directly from Eq. 32.

Having already obtained the mean, the second-order moment of $g_{N,ELT}$ can be obtained by following the steps used in the MLT domain analysis. As a result, the variance of $g_{N,ELT}$ may be written as [22]

$$\sigma_{g,ELT}^{2} \;=\; \frac{N_0}{2} \sum_{\mathcal{I}} \underline{C}_{\mathcal{I}}^{T} \mathrm{diag}(\underline{\alpha}_{\mathcal{I}}) \mathrm{diag}(\underline{\alpha}_{\mathcal{I}}) \underline{C}_{\mathcal{I}}.$$

This expression, together with Eq. 36, yields the probability of bit error,

$$P_{e,ELT} \;=\; \frac{1}{2\pi} \int_{0}^{2\pi} Q \left(\frac{\mu_{g,ELT|\theta}}{\sigma_{g,ELT}} \right) d\theta.$$

A receiver employing ELT domain excision and detection is shown in Figure 14. As in the case of MLT domain excision, each of the weighting vectors, $\underline{\alpha}_{\mathcal{I}}$, has binary valued elements, i.e. zero or unity, based on the interference energy distribution among the appropriate set of transform domain coefficients, $\underline{R}_{\mathcal{I}}$. Note that in this

36

figure, as in Figure 13, the spreading code is assumed to be purely real since only real signals and transforms are considered.

3.1.3 Gaussian Interference

In many applications, the narrow-band interference can be approximated by an equivalent narrow-band Gaussian process. For a given amount of interference power, the narrow-band Gaussian interferer affects a larger frequency range than a single-tone jammer but with lower power spectral density. Denoting the percentage of the spread signal bandwidth which is jammed as ρ and the total interference power as A_{nb}^2, the two-sided power spectral density of $j[n]$ is simply $\frac{A_{nb}^2}{2\rho}$. The corresponding jammer-to-signal ratio (JSR) is given by

$$JSR = \frac{A_{nb}^2}{P_s}.$$

Denoting the spread spectrum signal bandwidth as ω_{ss} and the jammer bandwidth as $\omega_{nb} = \rho\omega_{ss}$, the lower and upper cutoff frequencies of the narrow-band spectral response are defined as $\omega_1 \triangleq \delta\omega - \frac{\omega_{nb}}{2}$ and $\omega_2 \triangleq \delta\omega + \frac{\omega_{nb}}{2}$, respectively. With the narrow-band interference power spectral density given as

$$|J(\omega)|^2 = \begin{cases} \frac{A_{nb}^2}{2\rho} & \omega_1 \leq |\omega| \leq \omega_2 \\ 0 & \text{otherwise} \end{cases},$$

the corresponding elements of the covariance matrix, $\mathbf{K}_{JJ}$, are defined as

$$\mathbf{K}_{\underline{jj}}(m,n) = \frac{A_{nb}^2}{\rho} \frac{\sin\left[\frac{\omega_{nb}}{2}(n-m)\right]}{\pi(n-m)} \cos\left(\delta\omega|m-n|\right).$$

Assuming that the discrete-time sampling frequency is twice the spread spectrum bandwidth, i.e. $f_s = 2\omega_{ss}$, ω_{ss} is normalized to π.

In this case, since the interference term is zero-mean, the mean of the MLT domain decision variable becomes [22]

$$\mu_{g,MLT} = \sum_{\mathcal{I}} \underline{C}_{\mathcal{I}}^T \text{diag}(\underline{\alpha}_{\mathcal{I}}) \underline{C}_{\mathcal{I}},$$

37

with the associated variance given as

$$\sigma^2_{g,MLT} \;=\; \frac{N_0}{2} \sum_{\mathcal{I}} \underline{C}^T_\mathcal{I} \mathrm{diag}(\underline{\alpha}_\mathcal{I}) \mathrm{diag}(\underline{\alpha}_\mathcal{I}) \underline{C}_\mathcal{I} + \sum_{\mathcal{I}} \underline{C}^T_\mathcal{I} \mathrm{diag}(\underline{\alpha}_\mathcal{I}) \mathbf{K}_{JJ} \mathrm{diag}(\underline{\alpha}_\mathcal{I}) \underline{C}_\mathcal{I}.$$

Likewise, the mean and variance associated with the ELT domain decision variable are given by

$$\mu_{g,ELT} \;=\; \sum_{\mathcal{I}} \underline{C}^T_\mathcal{I} \mathrm{diag}(\underline{\alpha}_\mathcal{I}) \underline{C}_\mathcal{I}$$

and

$$\sigma^2_{g,ELT} \;=\; \frac{N_0}{2} \sum_{\mathcal{I}} \underline{C}^T_\mathcal{I} \mathrm{diag}(\underline{\alpha}_\mathcal{I}) \mathrm{diag}(\underline{\alpha}_\mathcal{I}) \underline{C}_\mathcal{I} + \underline{C}^T_\mathcal{I} \mathrm{diag}(\underline{\alpha}_\mathcal{I}) \mathbf{K}_{JJ} \mathrm{diag}(\underline{\alpha}_\mathcal{I}) \underline{C}_\mathcal{I},$$

respectively. Note that above, $\mathcal{I} \in \{I, II\}$ for the MLT and $\mathcal{I} \in \{I, II, III, IV\}$ for the ELT. The probability of bit error associated with the MLT and ELT domain excision systems can be obtained by substituting the appropriate mean and variance into

$$P_e = Q\left(\frac{\mu_g}{\sigma_g}\right).$$

3.2   Analytical and Simulated Results

In practice, since transform domain excision decisions are typically a function of the spectral distribution of the interfering signal's energy, many applications evaluate the magnitude of each transform domain bin and remove those that exceed a preset threshold. Such an excision scheme is easily implemented in hardware and is simply termed as "threshold excision". Unfortunately, the stochastic nature of the threshold excision process makes its analysis mathematically impractical. As a result, an analytically tractable excision scheme allowing objective evaluation of various linear transforms and filter banks is considered here.

To obtain the average probability of bit error, transform domain vectors corresponding to the received data signal with the k largest magnitude bins removed are

38

determined for several different phases of the interferer - this technique is referred to as the "k-bin" excision algorithm. Using these conditional vectors, the corresponding bit error probabilities are obtained and averaged over a large number of phases to obtain the final bit error rate expression. To simplify the analysis, the selection of the k bins to be excised is based solely on the transform domain distribution of the narrow-band interference energy; this approach is valid provided that relatively large JSR ratios are considered and that only a small percentage of bins are removed. Although not considered here, excision analysis may also be performed by determining the optimal number and location of bins to excise to minimize the probability of bit error for each phase [22].

Excision-based receivers using the MLT and the ELT have been shown previously in Figures 13 and 14, respectively. Although not explicitly shown in the receiver diagrams, the transform domain weighting vectors are based on the transform domain distribution of interference energy using the k-bin excision algorithm. Regarding the MLT domain excision process, the transform domain weighting vectors, $\underline{\alpha}_I$ and $\underline{\alpha}_{II}$, might be expected to be identical since each of the transform domain vectors, $\underline{R}_I$ and $\underline{R}_{II}$, are merely delayed replicas of one another. Due to the fact that the desired data bit energy is not equally divided among these transform domain representations, however, such an assumption is unwarranted and may lead to slightly less reliable results. Similar statements apply equally well when excision is performed in the ELT domain. Throughout this section, lapped transform domain excision vectors are based on the entire set of transform domain coefficients and evaluated simultaneously, thereby inherently taking into account the distribution of data bit energy throughout the transform domain.

In the following sections, analytical BER results illustrate the performance of spread spectrum receivers employing lapped transform domain excision in the presence of narrow-band interference. In each of the interference scenarios considered,
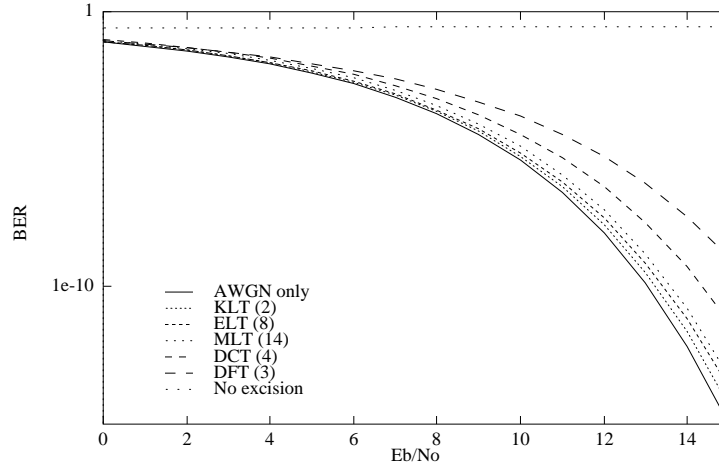
Figure 15: Excision in the presence of single-tone interference, JSR = 20 dB and $\delta\omega$ = 0.126984 rad/sec.

a 64-chip augmented spreading code is used to modulate the binary data. Consequently, the dimensionality of the transformation matrix is 64×64 for block transforms, 64×128 for the MLT and 64×256 when using the ELT. The ELT lowpass prototype filter is generated using $\gamma = 0.5$. In each case, the number of bins excised is indicated in parentheses in the figure legend.

3.2.1 Single-Tone Interference

Based on the analysis of Section 3.1, receiver performance using transform domain excision and a variety of orthonormal block transforms in the presence of a single-tone interferer with $\delta\omega = 0.126984$ rad/sec and JSR = 20 dB is shown in Figure 15. As in [22], the block and subband transforms tested include the DFT, DCT and the Karhunen-Loève transform (KLT); the number of transform domain bins excised in each case is shown parenthetically in the figure legend. As expected, the KLT, which confines the interfering sinusoids to two basis vectors, yields the best BER performance [22]. Among the fixed transform techniques considered, both lapped transforms produce results comparable to the KLT and significantly better than those
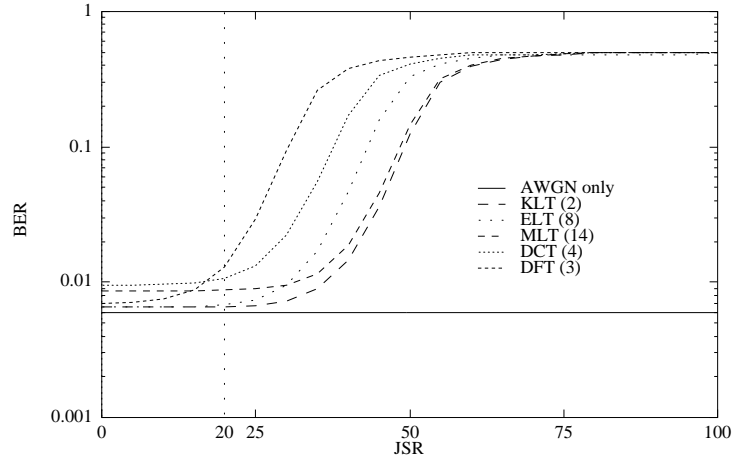
40

Figure 16: Excision in the presence of single-tone interference as a function of JSR, $E_b/N_0 = 5$ dB and $\delta\omega = 0.126984$ rad/sec.

achieved by most of the block transform implementations. In fact, with respect to the KLT performance results, the ELT and MLT bit error rates are within 0.2 dB and 0.4 dB, respectively, whereas the DCT generates the lowest BER of all the block transforms considered yet is roughly 1.2 dB worse.

As suggested in the design of the ELT lowpass prototype filters in Section 2.1.3, there is always a trade-off between the bandwidth of the main lobe and the level of attenuation in the sidelobes. Due to windowing effects and, thus, relatively poor attenuation in the sidelobes, the performance obtained using the DFT is rather poor for the given interference environment. In contrast, the lower BER associated with lapped transform domain excision can be attributed to the relatively small bandwidth and high stopband attenuation associated with the LT subband filters, a direct result of the longer basis vectors.

Figures 16 and 17 illustrate the performance of the excision-based receivers as a function of the JSR and $\delta\omega$, respectively. In Figure 16, the number of bins excised is held fixed as the jammer power is allowed to increase. In this figure, the KLT basis vectors have not been recalculated for each JSR value tested. Although the two
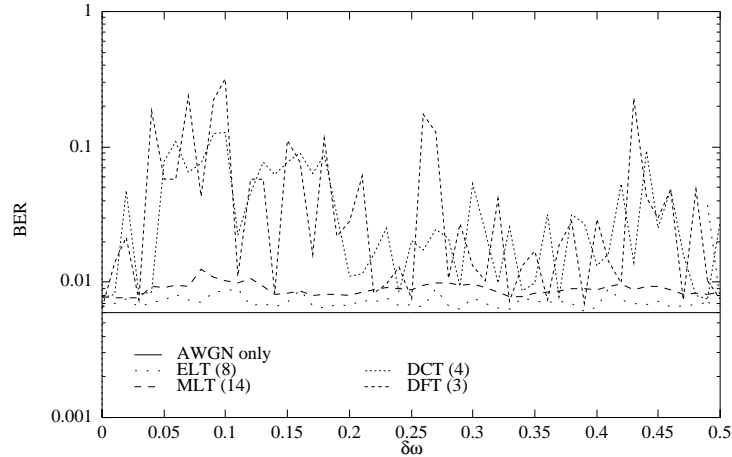
41

Figure 17: Excision in the presence of single-tone interference as a function of frequency, $E_b/N_0 = 5$ dB and JSR $= 20$ dB.

KLT basis vectors excised optimally characterize the interfering tone [22], as the JSR increases the interference energy present in the remaining basis vectors increases almost uniformly in each bin. As a result, the residual interference acts as a white noise source with its power commensurately related to that of the single-tone jammer. Due to the high levels of stopband attenuation associated with the lapped transforms, the MLT and ELT are capable of tolerating larger power interferers without significantly compromising performance. In fact, for both the MLT and ELT, relatively low BER results, i.e. less than 0.0095, are maintained up to a JSR of approximately 30 dB. As in practice, if the jammer power is sufficiently large, the excision process is rendered ineffective and alternative measures, such as coding or longer spreading codes, must be implemented.

Figure 17 illustrates the BER obtained as a function of jammer frequency offset, $\delta\omega$. In these figures, the KLT is not considered since it has been previously optimized only for $\delta\omega = 0.126984$ rad/sec. Here, the robustness of lapped transform domain excision relative to the jammer frequency is demonstrated as the performance of both the MLT and the ELT does not deviate significantly from the theoretical BER
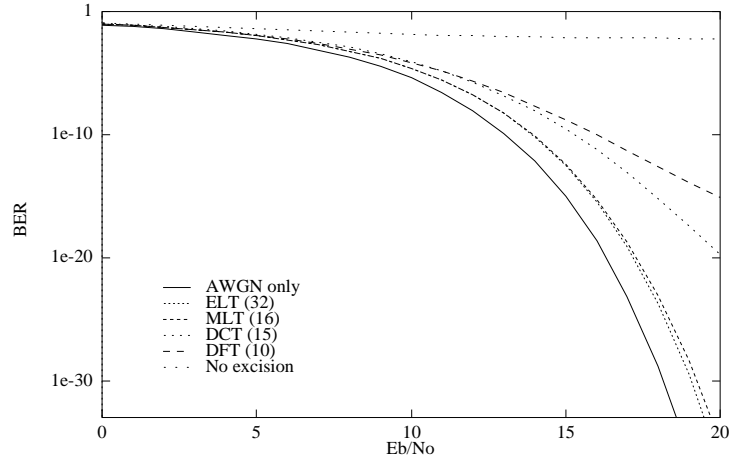
Figure 18: Excision in the presence of narrow-band Gaussian interference, JSR = 10 dB, $\delta\omega = 0.126984$ rad/sec and $\rho = 0.1$.

performance in AWGN over all frequencies. In contrast, the block transform implementations are highly sensitive to frequency. This sensitivity is once again a function of the frequency responses of the transform basis vectors.

3.2.2 Narrow-Band Gaussian Interference

In this section, the excision-based receivers are evaluated in the presence of narrowband Gaussian interference. As discussed in Section 3.1.3, the parameters characterizing this type of interferer are the JSR, the center frequency, $\delta\omega$, and the fractional bandwidth, ρ. Regarding the following results, $E_b/N_0 = 5$ dB, JSR = 10 dB, $\delta\omega = 0.126984$ rad/sec and $\rho = 0.1$ unless otherwise noted.

Figure 18 illustrates receiver performance as a function of E_b/N_0. As in the case of the single-tone interference shown in Figure 15, the best performance is obtained using the lapped transforms, which consistently yield BER results within $1.0 - 1.5$ dB of that obtained in AWGN alone; in contrast, all of the block transforms considered clearly produce substantially poorer results. Such performance results are rather impressive considering that the removal of 10% of the spread spectrum signal energy results in an
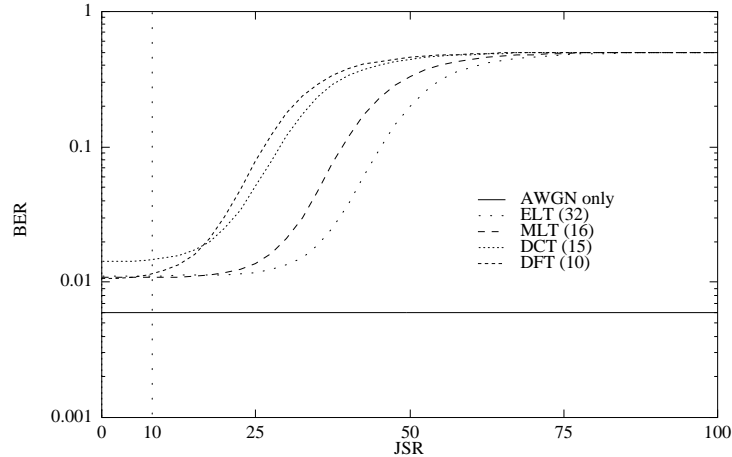
Figure 19: Excision in the presence of narrow-band Gaussian interference as a function of JSR, $E_b/N_0 = 5$ dB, $\delta\omega = 0.126984$ rad/sec and $\rho = 0.1$.

immediate loss of roughly 0.46 dB in performance. Although these results correspond to a very specific jamming environment, additional analytical and experimental results have verified that similar performance is achieved over all frequencies.

Figure 19 shows that the lapped transform domain excision schemes provide the best performance as the JSR increases. Note, however, that in this case, the ELT requires the same percentage of bins excised as the MLT and is slightly more tolerant of higher power jammers at this frequency. Although not shown, the MLT and ELT are, once again, less sensitive to jammer frequency than the block transforms considered [22].

4   Conclusions

The analysis presented herein establishes the optimal transform domain Wiener filter performance attainable using either block or lapped transforms. Although the concept of block transform domain Wiener filtering is not new, this work establishes a benchmark for BER performance in the presence of narrow-band interference and provides the groundwork for subsequent analysis of transform domain LMS algorithms

44

and the effects of their underlying transforms on such performance characteristics as convergence rate, misadjustment noise and BER. As shown in Figures 8 – 11, there is not much difference between the BER performance obtained using block and lapped transform domain Wiener filters. The fundamental advantage of transform domain Wiener filtering over conventional time domain approaches is in the potential improvement in convergence rates when adaptive algorithms are used [21].

As demonstrated above, transform domain excision performance is largely dependent on the transform's ability to compactly represent the interfering signal energy in the transform domain. To efficiently suppress narrow-band interference signals via excision, transforms with similarly narrow-band basis vectors are required. Theoretically, narrow-band interference is best removed using a uniform bank of bandpass filters with unity gain in the passband and infinite stopband attenuation. Of the transforms considered here and in [22], lapped transforms most closely approximate this ideal.

Herein, it has been shown that the lapped transform domain excision algorithms are relatively insensitive to jammer frequency. Such a characteristic is often advantageous in practice since one is seldom guaranteed that the frequency of the interfering tone is known or constant. Considering that these algorithms are also relatively insensitive to jammer power and that their complexity using polyphase filter bank structures rivals that of conventional block transform algorithms [19], the MLT and ELT must be considered as worthy transforms for narrow-band interference excision applications.

References

[1] S. Davidovici and E. G. Kanterakis. Narrow-band interference rejection using real-time Fourier transforms. *IEEE Transactions on Communications*, 37(7):713–722, July 1989.

[2] R. C. DiPietro. An FFT based technique for suppressing narrow-band interference in PN spread spectrum communications systems. In *IEEE ICASSP '89 Conference Record*, pages 1360–1363, 1989.

[3] R. C. Dixon. *Spread Spectrum Systems*. Wiley-Interscience, New York, 1976.

[4] B. Farhang-Boroujeny and S. Gazor. Selection of orthonormal transforms for improving the performance of the transform domain normalised LMS algorithm. *IEE Proceedings - F*, 139(5):327–335, October 1992.

[5] J. Gevargiz, P. Das, and L. B. Milstein. Performance of a transform domain processing DS intercept receiver in the presence of finite bandwidth interference. In *IEEE Global Telecommunications Conference '86 Conference Record*, pages 21.5.1–21.5.5, December 1986.

[6] J. Gevargiz, M. Rosenmann, P. Das, and L. B. Milstein. A comparison of weighted and non-weighted transform domain processing systems for narrowband interference excision. In *IEEE MILCOM '84 Conference Record*, pages 32.3.1–32.3.4, October 1984.

[7] R. F. Guertin. Narrowband interference suppression in a spread-spectrum system using vector space methods. In *IEEE MILCOM '89 Conference Record*, pages 28.5.1–28.5.5, 1989.

[8] S. S. Haykin. *Adaptive Filter Theory*. Prentice-Hall, Englewood Cliffs, New Jersey, 1986.

46

[9] J. K. Holmes. *Coherent Spread Spectrum Systems.* John Wiley & Sons, Inc., 1982.

[10] S. J. Howard. Narrowband interference rejection using small FFT block sizes. In *IEEE MILCOM '92 Conference Record*, pages 26.3.1–26.3.5, 1992.

[11] R. A. Iltis and L. B. Milstein. Performance analysis of narrow-band interference rejection techniques in DS spread-spectrum systems. *IEEE Transactions on Communications*, COM-32(11):1169–1177, November 1984.

[12] W. W. Jones and K. R. Jones. Narrowband interference suppression using filter-bank analysis/synthesis techniques. In *IEEE MILCOM '92 Conference Record*, pages 898–902, October 1992.

[13] J. W. Ketchum and J. G. Proakis. Adaptive algorithms for estimating and suppressing narrow-band interference in PN spread-spectrum systems. *IEEE Transactions on Communications*, COM-30:913–924, May 1982.

[14] R. D. Koilpillai and P. P. Vaidyanathan. Cosine-modulated FIR filter banks satisfying perfect reconstruction. *IEEE Transactions on Signal Processing*, 40:770–783, April 1992.

[15] J. C. Lee and C. K. Un. Performance of transform domain LMS adaptive digital filters. *IEEE Transactions on Acoustics, Speech, and Signal Processing*, ASSP-34(3):499–510, June 1986.

[16] L. M. Li and L. B. Milstein. Rejection of narrow-band interference in PN spread-spectrum systems using transversal filters. *IEEE Transactions on Communications.*, COM-30:925–928, May 1982.

[17] H. S. Malvar. Lapped transforms for efficient transform/subband coding. *IEEE Transactions on Acoustics, Speech, and Signal Processing*, ASSP-38(6):969–978, June 1990.

[18] H. S. Malvar. Modulated QMF filter banks with perfect reconstruction. *Electronics Letters*, 26:906–907, June 1990.

[19] H. S. Malvar. *Signal Processing with Lapped Transforms*. Artech House, Boston, 1992.

[20] H. S. Malvar and D. H. Staelin. The LOT: Transform coding without blocking effects. *IEEE Transactions on Acoustics, Speech, and Signal Processing*, ASSP-37(4):553–559, April 1989.

[21] D. F. Marshall, W. K. Jenkins, and J. J. Murphy. The use of orthogonal transforms for improving performance of adaptive filters. *IEEE Transactions on Circuits and Systems*, CAS-36(4):474–484, April 1989.

[22] M. J. Medley. *Adaptive Narrow-band Interference Suppression Using Linear Transforms and Multirate Filter Banks*. PhD thesis, Rensselaer Polytechnic Institute, December 1995.

[23] M. J. Medley, G. J. Saulnier, and P. K. Das. Radiometric detection of direct-sequence spread spectrum signals with interference excision using the wavelet transform. In *IEEE ICC '94 Conference Record*, pages 1648–1652, May 1994.

[24] M. J. Medley, G. J. Saulnier, and P. K. Das. The application of wavelet-domain adaptive filtering to spread spectrum communications. In H. Szu, editor, *SPIE Proceedings - Wavelet Applications for Dual-Use*, volume 2491, pages 233–247, April 1995.

[25] M. J. Medley, G. J. Saulnier, and P. K. Das. Convergence analysis and misadjustment in transform domain LMS algorithms. *IEEE Transactions on Signal Processing*, 1997. to be submitted.

[26] M. J. Medley, G. J. Saulnier, and P. K. Das. Narrow-band interference excision in spread spectrum systems using lapped transforms. *IEEE Transactions on Communications*, COM-45(11):1444–1455, November 1997.

[27] M. Mettke, M. J. Medley, G. J. Saulnier, and P. K. Das. Wavelet transform excision using IIR filters in spread spectrum communication systems. In *IEEE Globecom '94 Conference Record*, pages 1627 – 1631, November 1994.

[28] L. B. Milstein and P. K. Das. An analysis of a real-time transform domain filtering digital communication system - Part I: Narrowband interference rejection. *IEEE Transactions on Communications*, COM-28(6):816–824, June 1980.

[29] L. B. Milstein and P. K. Das. An analysis of a real-time transform domain filtering digital communications system - Part II: Wideband interference rejection. *IEEE Transactions on Communications*, COM-31:21–27, June 1983.

[30] L. B. Milstein, P. K. Das, and J. Gevargiz. Processing gain advantage of transform domain filtering DS-spread spectrum systems. In *IEEE MILCOM '82 Conference Record*, pages 21.2.1–21.2.5, November 1982.

[31] L. B. Milstein, S. Davidovici, and D. L. Schilling. The effect of multiple-tone interfering signals on direct sequence spread spectrum communication system. *IEEE Transactions on Communications*, COM-30(3):436–446, March 1982.

[32] S. S. Narayan, A. M. Peterson, and M. H. Narasimha. Transform domain LMS algorithm. *IEEE Transactions on Acoustics, Speech, and Signal Processing*, ASSP-31(3):609–615, June 1983.

[33] T. Q. Nguyen. A quadratic-constrained least-squares approach to the design of digital filter banks. In *IEEE International Symposium on Circuits and Systems '92 Proceedings*, pages 1344–1347, San Diego, May 1992.

[34] T. Q. Nguyen. The design of arbitrary FIR digital filters using the eigenfilter method. *IEEE Transactions on Signal Processing*, 41(3):1128–1139, March 1993.

[35] C. N. Pateros and G. J. Saulnier. An adaptive correlator receiver for direct-sequence spread-spectrum communication. *IEEE Transactions on Communications*, 44(11):1543–1552, November 1996.

[36] J. Patti, S. Roberts, and M. Amin. Adaptive and block excisions in spread spectrum communication systems using the wavelet transform. In *The Conference Record of the 28th Asilomar Conference on Signals, Systems and Computers*, pages 293–297, Pacific Grove, CA, November 1994.

[37] T. A. Ramstad. Cosine modulated analysis-synthesis filter bank with critical sampling and perfect reconstruction. In *IEEE ICASSP '91 Conference Record*, pages 1789–1792, Toronto, Canada, May 1991.

[38] R. Rifkin. Comments on "Narrow-band interference rejection using real-time Fourier transforms". *IEEE Transactions on Communications*, 39(9):1292–1294, September 1991.

[39] M. Rosenmann, J. Gevargiz, P. Das, and L. B. Milstein. Probability of error measurement for an interference resistant transform domain processing receiver. In *IEEE MILCOM '83 Conference Record*, pages 638–640, October 1983.

[40] S. D. Sandberg. Adapted demodulation for spread-spectrum receivers which employ transform-domain interference excision. *IEEE Transactions on Communications*, 43(9):2502–2510, September 1995.

[41] S. D. Sandberg, S. Del Marco, K. Jagler, and M. A. Tzannes. Some alternatives in transform-domain suppression of narrow-band interference for signal detection and demodulation. *IEEE Transactions on Communications*, 43(12):3025–3036, December 1995.

[42] G. J. Saulnier, P. Das, and L.B. Milstein. An adaptive digital suppression filter for direct sequence spread spectrum communications. *IEEE Journal on Selected Areas in Communications*, SAC-3(5):676–686, September 1985.

[43] M. V. Tazebay and A. N. Akansu. Adaptive subband transforms in time-frequency excisers for DSSS communications systems. *IEEE Transactions on Signal Processing*, 43(11):2776–2782, November 1995.

[44] P. P. Vaidyanathan and T. Q. Nguyen. Eigenfilters: A new approach to least-squares FIR filter design and applications including Nyquist filters. *IEEE Transactions on Circuits and Systems*, CAS-34(1):11–23, January 1987.

[45] B. Widrow and S. D. Stearns. *Adaptive Signal Processing*. Prentice-Hall Signal Processing Series. Prentice-Hall, Englewood Cliffs, New Jersey, 1985.